Winter 2012

Study of electrocatalysis for direct alcohol fuel cells (DAFC)

Ryan S. Banfield
University of New Hampshire, Durham

STUDY OF ELECTROCATALYSIS FOR DIRECT ALCOHOL FUEL CELLS (DAFC)

By

Ryan S Banfield
B.S. University of New Hampshire, 2006

THESIS

Submitted to the University of New Hampshire
In partial fulfillment of
the requirements for the Degree of

Master of Science
In
Chemical Engineering

December 2012

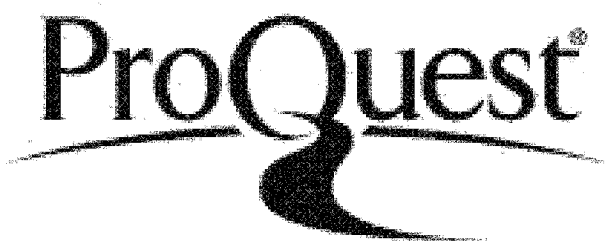

ProQuest LLC
789 East Eisenhower Parkway
P.O. Box 1346
Ann Arbor, MI 48106-1346

This thesis has been examined and approved.

Virendra K. Mathur

Thesis Director, Virendra K. Mathur, Professor of Chemical Engineering

Gupta

Nivedita Gupta, Associate Professor of Chemical Engineering

Xiaowei Teng, Assistant Professor of Chemical Engineering

October 1, 2012

Date

Acknowledgements

I would like to thank Dr. Mathur for his dedication and continued support of my work. Without him the completion of this study would not have been possible.

I would also like to thank Dr. N. Gupta, Dr. X. Teng for their participation in reviewing this work. Additional thanks to Dr. P. Vasudevan for his support throughout my time as an Undergraduate and Graduate student.

I am also very grateful to my parents for their continued support and pride in my work and accomplishments.

Table of Contents

List of Figures

List of Tables

Abstract

STUDY OF ELECTROCATALYSIS FOR DIRECT ALCOHOL FUEL CELLS (DAFC)

By

Ryan Banfield

University of New Hampshire, December 2012

Under this work an automated 5 inch single-cell PEM fuel cell was retrofitted with a computer controlled syringe pump and operated as a DAFC. Catalyst synthesis procedures were developed in-house for DAFC catalysts preparations. Six catalysts, PtSn/C, Pt_2Sn/C, Pt_2SnRu/C, $PtSnRu_{0.5}/C$, $PtSn_{0.5}Ru/C$ and Pd/C were prepared, and their mass composition estimated through mass balance calculations. A series of experiments for VI performance data and power output were performed in the DAFC at different temperatures (75°C, 80°C, 85°C) and 1M ethanol flow rates(0.32ml/min, 1ml/min, 2ml/min) with a fixed catalyst loading of $1mg/cm^2$ platinum. It was found that the binary platinum-tin catalysts produced about 18% more power than the ternary platinum-tin-ruthenium catalysts in the DAFC.

Chapter 1 : Introduction

Energy production is vital to today's society. Currently, a majority of the electricity produced is derived from coal, oil and natural gas; all fossil fuels. Combusting these fuels not only dwindles their finite supply, but is inefficient, and polluting. Alternatives exist. Nuclear power is incredibly promising, but faces too many political and social hurdles, in addition to the potentially catastrophic dangers associated with its use. Geothermal is unique to one location only. Hydroelectric power is at its limit in most places. Wind energy is gaining popularity, but growth is limited by location and conflict of public interest. Photovoltaic cells and batteries have seen many innovative advancements recently, but are still inefficient and expensive. An alternative solution to both stationary and automotive power production are fuel cells.

A fuel cell is an electrochemical device that can directly convert the chemical energy produced by a fuel and oxidant into electricity without the efficiency limitations of the Carnot cycle inherent to internal combustion engines (ICEs). When the fuel and oxidant are hydrogen and air, the only byproducts are water and nitrogen. A fuel cell can be thought of as a battery, only unlike a battery, the reactants flow continuously, and as long as they are supplied, there is no interruption in the power produced. Even with the advantage of higher efficiency, and nearly pollution-free operation, the costs of a fuel cell system and hydrogen hold it back from commercialization. However, the discoveries of natural gas deposits in Pennsylvania and NY State could lead to a drastic

reduction in hydrogen costs, giving fuel cells their first opportunity to compete in the consumer market. The hydrogen fuel cell was first stumbled upon in 1839 by William Grove, and has since then been developed and improved [1].

Several types of fuel cells exist and differ by the catalyst, reactants and operating temperatures used. They are classified by their electrolytes. The most promising types are polymer exchange membrane fuel cells (PEMFCs), alkaline fuel cells(AFCs), direct alcohol or methanol fuel cells (DAFCs, DMFCs), solid oxide fuel cells (SOFCs), regenerative fuel cells, and moleten carbonate fuel cells (MCFCs). MCFCs and SOFCs operate at temperatures between 600-1000°C and are well-suited for stationary power generation. AFCs can operate at a relatively low temperature of 90°C, but require an ultra-pure source of hydrogen, reducing their practicality.

This study uses a PEMFC operating with hydrogen and alcohols (methanol and ethyl alcohol). At the heart of a PEMFC is a five-layer membrane electrode assembly (MEA). The assembly is made up of two gas diffusion layers (GDLs), two catalyst layers (typically platinum supported on carbon for hydrogem PEMFCs), and a proton conducting Nafion® membrane. The GDLs allow for fuel and oxidant to diffuse to the membrane, at the same time allowing for water produced at the cathode (oxidant side) to be removed quickly from the catalyst layer. The catalyst layer aids in reaction kinetics, and accelerates the hydrogen oxidation reaction (HOR) on the anode, and oxygen reduction reaction (ORR) on the cathode. The HOR produces protons which are conducted through the Nafion® membrane, while the free electrons are available for electrical work. At

the cathode the free electrons, oxygen and hydrogen combine to form water molecules.

PEMFCs, DAFCs and DMFCs operate at a low temperature (<90°C), and use a thin, solid polymer electrolyte, making them ideal for widespread use in small electronic devices as well as automobiles. Oxidants are typically air or oxygen, and with complete reactions, the primary byproducts are CO_2 and H_2O for alcohol-based fuel cells and water for hydrogen-based PEMFCs. Direct alcohol fuel cells differ from hydrogen fueled PEMFCs in that instead of a gaseous hydrogen fuel, liquid alcohol is pumped into the fuel cell. In DMFCs, the alcohol is methanol, in DAFCs, the alcohol is ethanol (ethyl alcohol). While hydrogen PEMFCs produce electricity cleanly, with water as the only byproduct, their practicality is hindered by difficult storage, transportation and cost of hydrogen. The liquid fuel for direct fuel cells makes transportation and storage much more practical. In the case of methanol, the increased practicality is offset by its extreme flammability and toxicity.

Toxicity aside, DMFC research has shown methanol to be a competitive fuel, with power densities of as high as 150mW/cm^2 measured at the University of New Hampshire fuel cell lab using DMFC optimized components [2]. The simple structure of methanol gives it a kinetic advantage compared to the more complex and stable ethyl alcohol. The simplicity of methanol makes the fuel prone to crossover, which is the transport of fuel from the anode to the cathode of the fuel cell without methanol oxidation, reducing the power produced. Anode kinetics aside, methanol crossover is the largest hurdle for DMFCs. While

methanol and ethanol can be processed from biological feed stocks in potentially carbon-neutral processes, the safety concerns and energy densities (19.9MJ/kg for methanol, 26.8MJ/kg for ethanol) make ethanol a more promising fuel [3]. The complex and slow electro-oxidation kinetics of ethanol are what prompted this and many other studies [4, 5, 6, 7, 8, 9, 10, 11, 12].

The major problems with DAFC performance are similar to the problems DMFCs faced several years ago. Ethanol fuel crossover, two-phase flow at the anode diffusion layer, and slow anode kinetics prevent DAFCs from achieving the same level of performance that has been seen with DMFCs. To improve DAFC performance, ustom membranes to control ethanol crossover, and GDLs to manage the two-phase flow need to be designed and researched. Presently, the primary hurdle to DAFC performance is anode kinetics. The issue lies in the multi-step mechanism for ethanol electro-oxidation, requiring multiple byproducts to be oxidized to carbon dioxide. The current focus in DAFC research is to improve the anode catalysts to achieve more effective fuel use and ensure complete oxidation of ethanol.

Cost is another major factor preventing a widescale commercialization and adoption of fuel cells. Companies like Nuvera Fuel Cells and Plug Power have attempted to gain traction in the industrial forklift market with fuel cell systems that replace the large, slow recharging batteries. Still, every component is an expensive hurdle, the GDL, catalyst, membrane and fuel. Ballard Material Products has recently begun production of GDLs with a continuous manufacturing process. Work funded by the U.S. Department of Energy is

focused on improving the ratio of power per milligram Pt required. Toyota and Gore are both researching thinner membranes that would reduce internal fuel cell resistance, increase performance, and reduce membrane material cost. With all of these advances, fuel still remains a high cost, and a commercialization inhibitor. With the recent discoveries of natural gas in the northeast, more affordable methanol, ethanol, and hydrogen are very possible.

The goal of this study is to investigate the use of ethanol as a fuel in PEM-based fuel cells, and to introduce a basic catalyst synthesis procedure to the University of New Hampshire fuel cell program in the Department of Chemical Engineering. At the time of this study, ongoing PEM fuel cell research was performed on hydrogen/air and DMFC fuel cells using two built in-house fuel cell systems. Each system consists of a $5cm^2$ single cell fuel cell connected to a computer using custom LabView® program for automated control and data acquisition. The work under this thesis includes the development of a catalyst synthesis procedure, characterization of the catalysts synthesized, and the evaluation of the synthesized catalysts in a DAFC.

Chapter 2 : Literature Review

This literatrure review is limited to the materials and processing that directly pertain to the subject matter of this study.

The hydrogen fuel cell is a promising technology. It is an electrochemical device that can directly convert the chemical energy produced by a fuel and oxidant into electricity. The Polymer Electrolyte Membrane(PEM) fuel cells can achieve thermal efficiencies of as much as 85%. Many obstacles stand in the way of the acceptance of fuel cells for commercial use. Specifically speaking, the cost of the fuel cell is very high. While some of the mechanical components are inexpensive, a hydrogen fuel cell uses a platinum based catalyst. Hydrogen is also a costly fuel. One of the biggest hurdles in the advancement of a hydrogen economy is an economically and environmentally feasible hydrogen source. Hydrogen is not naturally available as H_2. The most commonly practiced method of hydrogen production is the reforming of fossil fuels like natural gas(methane), gasoline, and diesel, as well as reforming of methanol. Electrolysis of water is another alternative, but is more costly. Recent discoveries of methane deposits in Pennsylvania and NY State could lead to a drastic reduction in hydrogen costs, and open the door to a viable hydrogen market. Still, hydrogen production is primarily fossil fuel dependent.

Methanol can be made from renewable sources, but has a high toxicity compared to ethanol. In light of the disadvantages of hydrogen and methanol, bio-ethanol is a viable alternative. It can be made locally from plants, grains,

waste materials. Ethanol(Ethyl alcohol) can be stored and transported safely and easily and has been used as an additive to gasoline in the US for many years. If necessary, bio-ethanol can be steam reformed into hydrogen, used in a combustion engine, or converted directly to electricity in a fuel cell. When manufactured from a truly renewable source, like switchgrass or cellulose, ethanol has the potential to be a CO_2 neutral fuel.

One molecule of ethanol generates 12 electrons (for every mole oxidized) whereas for hydrogen, 2 electrons are generated per mole oxidized. This gives ethanol an energy density of 56,8521 BTU per ft^3 based on its lower heating value(LHV) compared to an energy density of 68,000BTU per ft^3 for hydrogen [3]. Ethanol has the potential to be a much more practical fuel for PEM fuel cells, but several hurdles need to be removed before it can even be considered a rival to hydrogen. Due to incomplete oxidation of ethanol, chemical compounds such as carbon monoxide, acetaldehyde and acetic acid are formed, creating harmful waste and poisoning the fuel cells catalyst [7]. Additionally, Nafion® membrane, is susceptible to ethanol crossover, which severely limits fuel utilization. To combat incomplete electrochemical combustion more effective catalysts need to be synthesized with an emphasis on complete electrooxidation of ethanol. Preventing fuel crossover may require the development of composite membranes for specific use of ethanol, or the use of specialized gas diffusion layers with optimized micro porous layers for water and fuel management.

2.1 Catalysts and their role in Fuel Cells

A catalyst is a material that accelerates the rate of a reaction without itself being consumed in the process[13]. In alcohol fuel cells, catalysts are necessary to split oxygen molecules at the cathode, and break down the complex fuels at the anode. The most common catalyst for any PEM fuel cell is Pt, and it is typically supported on XC-72 Carbon. The support provides a high surface area for catalyst dispersion, while maintaining good electrical conductivity. While Pt alone is enough for hydrogen based PEM fuel cells, in the case of ethanol, a secondary, or sometimes ternary catalyst is required [7].

The most common secondary metals used in alcohol fuel cells as anode catalysts are ruthenium(Ru) and tin(Sn). The secondary metals improve the yield of the anodic reaction by oxidizing intermediates adsorbed on active sites of Pt catalyst. In Direct Alcohol Fuel Cells(DAFCs), the most abundant intermediates are carbon monoxide, acetic acid and acetaldehyde [7]. The secondary metal can form an alloy with Pt given a particular preparation method. Alloying changes the surface characteristics of a catalyst by creating a 2-dimensional alloy metal at the surface of the catalyst[13]. Alloying can affect the selectivity of a catalyst towards a specific product. The current focus of research for DAFC catalysts is to improve fuel usage through complete oxidation of intermediate species.

2.1.1 Tin as a DAFC Catalyst

Understanding the role of tin and other metals is critical in developing a highly effective catalyst for DAFCs. The study by Kim et al.[14] found the addition of Sn modified Pt , producing surface oxygenated species which might act as an oxidant source, increasing catalysts stability by improving oxidation of surface poisoning species. The study further found Sn sites were free to supply adsorbed OH, since CO did not tend to bind with Sn surface sites[14]. This is supported in literature by several authors. Wu et al.[5] studied PtRuSn/C catalysts in various mass ratios and found the Sn rich catalyst containing SnO_2 structures, made it more active toward C-C bond breakage. They were able to break C-C bonds in acetic acid which Ru rich catalysts were unable to do[5]. The formation of SnO_2 appears to be crucial in facilitating the oxidation of adsorbed CO species[10, 11, 15]. The oxide further improved the catalyst ability to dissociate water at low potentials, forming hydroxyl groups which were necessary in the oxidation of adsorbed species[16].

Even with the improved activity of Pt-Sn catalysts toward C-C bond breaking, the main reaction products are still acetic acid and acetaldehyde, which cause slower reaction kinetics and incomplete oxidation of ethanol to water and CO_2[17,18]. Wang et al.[17] report CO_2 representing around ~1% of the products of ethanol electrooxidation for bimetallic PtSn or PtRu catalysts measured by differential electrochemistry mass spectrometry(DEMS). Table 2.1 is presented by Rousseau et al.[7] suggests CO_2 production to be slightly higher when working with bimetallic and ternary based PtSn catalysts in a fuel cell system.

Table 2.1: Comparison of ethanol electrooxidation reaction products, Acetic Acid(AA) and Acetaldehyde(AAL), for different catalysts[7]

Catalyst	AA/Products(%)	AAL/Products(%)	CO_2/Products(%)
Pt/C XC72 60wt%	32.5	47.5	20.0
Pt-Sn(9:1)/C XC72 60wt%	76.9	15.4	7.7
Pt-Sn-Ru(86:10:4)/C XC72 60wt%	75	15.2	9.8

Colmati et al.[19] studied the effect of temperature on the mechanism for ethanol oxidation using carbon supported Pt, PtRu and Pt_3Sn electrocatalysts. For temperatures below 70°C, PtRu and Pt_3Sn perform similarly, and at T>70°C, Pt_3Sn catalyst performed better in a DAFC. The presence of Sn alloy allows ethanol to absorb dissociatively, breaking C-C bonds at lower potentials compared to Pt or PtRu catalysts[19].

While many workers agree that the addition of Tin and Ruthenium to Pt catalysts is the best starting point for the development of a DAFC specific catalyst, the optimum composition is still unknown, with many reporting similar performance results with non-similar catalyst compositions. There is also the issue of a lack of uniformity among testing methodology. The majority of the published work on the topic of ethanol electrooxidation and DAFCs do not test

catalysts in a DAFC system, rather they evaluate them at the half cell level. Half cell testing provides good insight into the performance of a catalyst in a fuel cell, but does not tell the whole story. Guo et al. also studied Pt_3Sn/C in a half cell and measured a maximum current of 16.2mA.[20]

Xue et al. [21] compared five Pt_3Sn_1/C catalysts using three different preparation methods. Through these preparations, they found that phosphorous can be deposited on the surface of the carbon support. They found the best composition to be $Pt_3Sn_1P_2/C$, which showed high activities compared to a Pt_3Sn_1/C catalyst prepared using ethylene glycol reduction or borohydride reduction preparation methods. Using a single cell at 70°C, 2.0M ethanol and pure oxygen at 2atm backpressure, they measured a maximum power density of 61mW/cm^2; 150 and 170% greater than that of PtSn catalysts prepared by ethelyne glycol reduction and borohydride reduction methods, respectively[21].

2.1.2 Ruthenium as a DAFC Catalyst

The addition of ruthenium(Ru) has been shown to increase activity of the catalysts toward ethanol electrooxidation, but typically the distribution of byproducts is unaffected[7]. This increase in activity may be due to the ability of Ru to remove C_1 and C_2 species from Pt sites at low potentials[5].

An optimized Ru loading has not yet been suggested, but Spinace et al.[6] have observed an increase in catalytic performance with an increase in Ru content. The relationship between Ru and Pt content was studied further and it

was found that for situations where low current density is drawn, a lower atomic % of Ru is favored, while the opposite is true for situations where high current density is drawn[22]. Liu et al.[23] found the Pt:Ru ratio of 52:48 gave the highest DAFC performance with a peak power density of 61mW/cm^2, and proposed the following reaction mechanism[23].

$$\mathbf{Pt\text{-}Ru\text{-}OH_{ad} + Pt\text{-}Ru{=}C{=}O \rightarrow 2Pt\text{-}Ru = CO_2 + H^+ + e^-} \quad (2.1)$$

$$\mathbf{2Pt\text{-}Ru\text{-}OH_{ad} + (CH_3\text{-}COOH)_{ads} \rightarrow 2Pt\text{-}Ru + 2CO_2 + 6H^+ + 6e^-} \quad (2.2)$$

Here, adsorbed hydroxyl(OH) groups react with carbon monoxide(CO) bound to PtRu sites to form carbon dioxide(CO_2), a proton and an electron in Equation 2.1. Equation 2.2 describes the reaction of adsorbed OH groups with acetic acid(CH_3-COOH) to form CO_2, a proton and electron. This mechanism describes one way complete oxidation of intermediates formed in a DAFC may occur.

2.1.3 Composition of PtSn Catalyst

It is still unclear as to what atomic ratio of Pt:Sn offers the best performance. Simoes et al.[18] prepared a table comparing different PtSn/C catalyst compositions and their peak performance values in a DAFC. Open Circuit Voltage(OCV) in Table 2.2 is defined later in Chapter 3.

Table 2.2: Comparison of catalyst performance in a DAFC at 110°C[18]

Catalyst	OCV(V)	Current Density (mA/cm^2)	Power Density (mW/cm^2)
PtSn/C(90:10)	0.81	160.1	71.8
PtSn/C(80:20)	0.79	120	51.8
PtSn/C(70:30)	0.81	180.1	55.7
PtSn/C(60:40)	0.77	159.9	49
PtSn/C(50:50)	0.76	140.6	42.3
Pt/C	0.5	60	7.5

The $72mWcm^{-2}$ peak power density achieved using a Pt:Sn ratio of 90:10, is the highest value in literature for direct alcohol fuel cells. The high operating temperature of 110°C may have something to do with that. The concern with these results is that Nafion membrane cannot be used reliably for extended periods of time at such a high operating temperature. The same Pt:Sn ratio was studied by Rousseau et al.[7], but observed a peak power density of only $28mW/cm^2$ at 80°C. This may be due to lower operating temperature. Here, a minimal amount of Sn is required to achieve high performance, while another study by Tsiakars et al.[24] has shown Sn content to be optimum between 35-40%[24]. The same study measured a peak power density of $65mW/cm^2$ in a DAFC with Pt_2Sn/C catalyst. A comparison of peak power output vs Sn composition, is shown in Figure 1. The second highest reported power density is $61mW/cm^2$ measured by Xue et al[21]. Their study involved the examination of

various PtSn/C catalysts. Their peak result of 61mW/cm^2 was achieved using $Pt_3Sn_1P_2$/C catalyst in a single fuel cell at 70°C, with a 2.0M ethanol fuel and pure oxygen at 2atm backpressure.

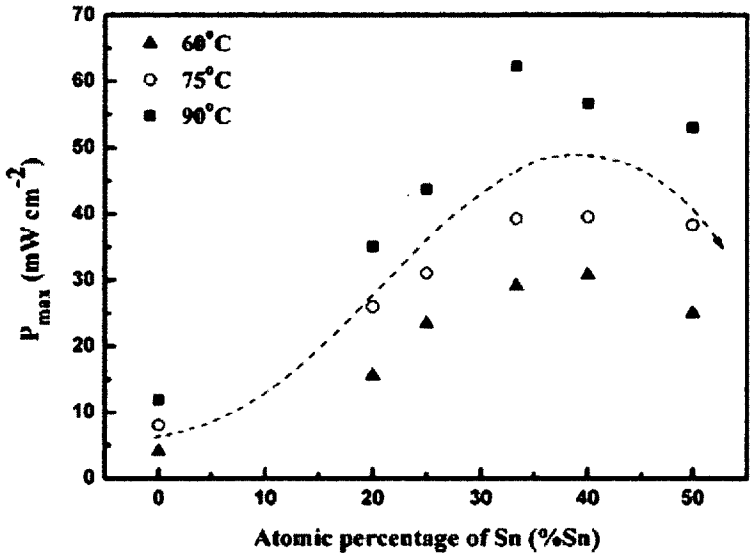

Figure 2.1: Maximum power density vs atomic % Sn in a DAFC[24].

Ternary catalysts(typically PtSnRu) have shown to be the most promising candidates for DAFCs[16]. The Pt-Sn alloys are capable of C-C bond breakage, while Ru assists in CO removal. Rousseau et al.[7] observed a peak power density of ~50mW/cm^2 with PtSnRu/C(86:10:4). Their study provided comparable performance data for binary and ternary DAFC catalysts, and the results are shown in Table 2.1[7]. Another study showed the optimal Pt:Ru:Sn atomic ratio to be 60:10:30, suggesting PtSn alloys and SnO_2 structures present in the catalyst improved the performance[11]. These results were also seen by Zhou et al. [15], where Pt was in a primarily metallic state, and Sn was primarily

in oxidized form. The results of their study suggested that optimal catalyst compositions existed for different operating temperatures.

2.1.4 Proposed Mechanisms for Ethanol Electrochemical Oxidation[14]

To understand the role of a catalyst and how it influences reaction products, the mechanisms for ethanol oxidation, and the oxidation of reaction byproducts need to be understood. The following are proposed reaction mechanisms for the reactions that occur in DAFCs.

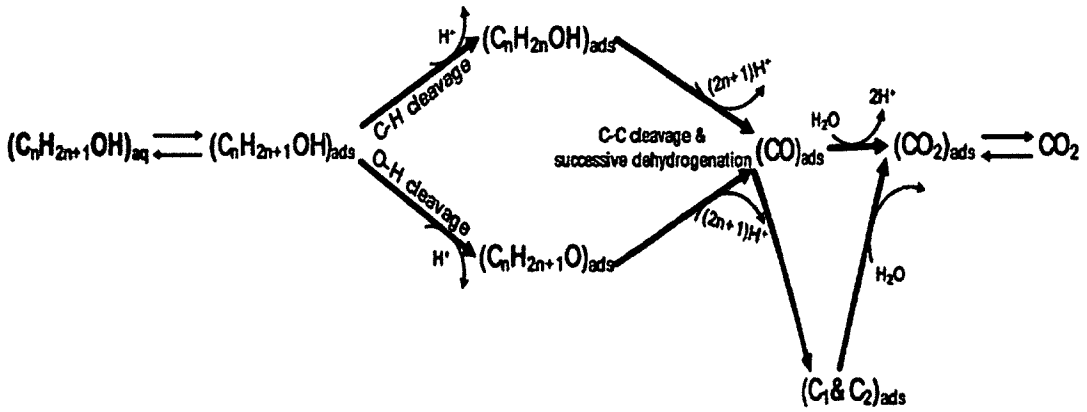

Figure 2.2: Proposed mechanism for C1-C3 alcohol oxidation to CO_2[14]

Figure 2.2 describes a reaction mechanism for oxidation of ethanol to CO_2 and C_1 and C_2 byproducts. First, ethanol is adsorbed onto the catalyst surface, where it can undergo hydrogen or hydroxyl group cleavage. The products are then adsorbed onto catalyst active sites and undergo carbon-carbon bond cleavage and dehydrogenation, forming adsorbed carbon monoxide. The carbon monoxide can be oxidized to carbon dioxide, or form C_1 and C_2 products. The

oxidation of the products forms CO_2. This mechanism assumes complete oxidation of ethanol to CO_2, an ideal assumption.

Figure 2.3 provides a graphical mechanism for reaction pathways on bimetallic PtSn electrocatalysts. Alcohol is first adsorbed onto the Pt surface where it undergoes oxidative clevage of H^+. The remaining C_1 and C_2 compounds undergo C-C bond cleavage after they are dehydrogenated. The figure shows the role of tin as it adsorbs hydroxyl groups from solution to aid in the oxidation of intermediates.

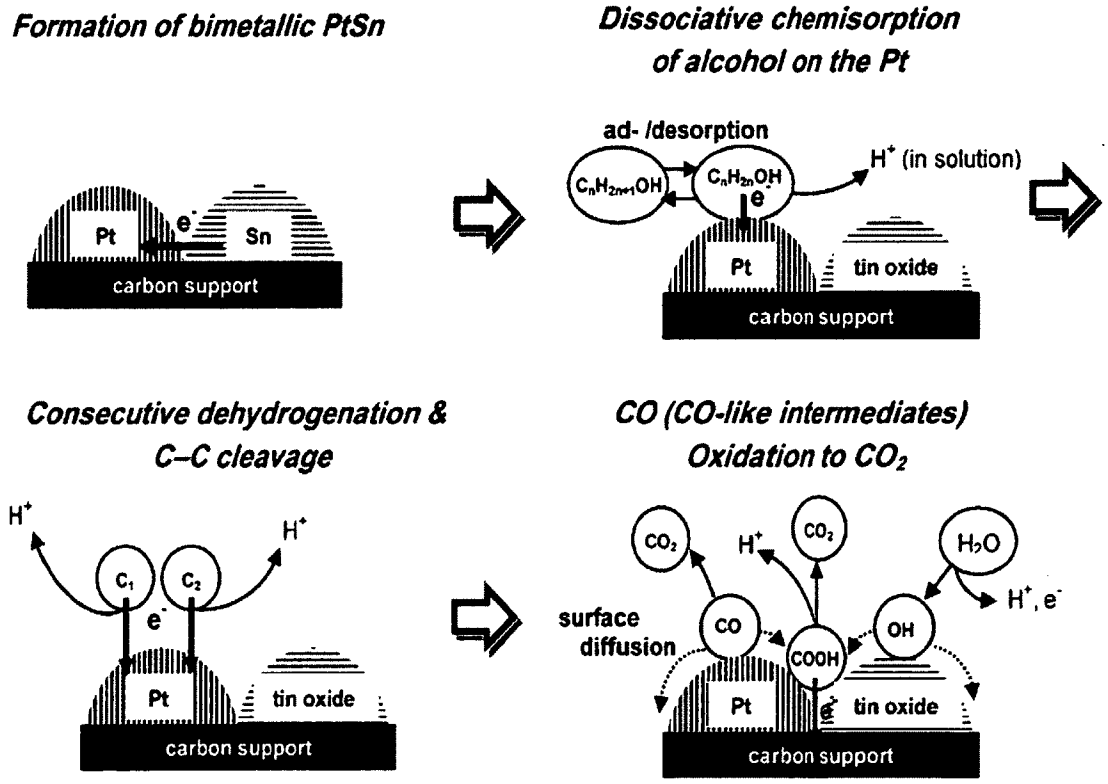

Figure 2.3:Possible reaction pathways over PtSn catalyst for C1-C3 oxidation[14]

Simoes et al.[18] proposed a similar, but more indepth ethanol oxidation scheme for alcohol electrooxidation on Pt-Sn catalysts, shown in Figure 2.4. The scheme is labeled in steps, 1-11. The first step is the assumed adsorption of ethanol on the surface of platinum, followed by C-H dissociation(step 2), forming acetaldehyde which is released into solution. Acetaldehyde is re-adsorbed in step 3, where it reacts with adsorbed OH, forming acetic acid(step 4). Acetic acid can also be formed by steps 5 and 6, but the authors note it is less probable. Steps 7-10 explain the presence of adsorbed CO. This requires C-H bond cleavage from both carbon bonds, as shown in step 7, and then subsequent C-C bond breakage in step 8. The second possibility is through steps 9 and 10, where the adsorbed acetaldehyde undergoes C-H bond cleavage(step 9), and subsequent C-C bond breakage(step 10). Finally, in step 11, the adsorbed CO species can react with adsorbed OH to form CO_2.

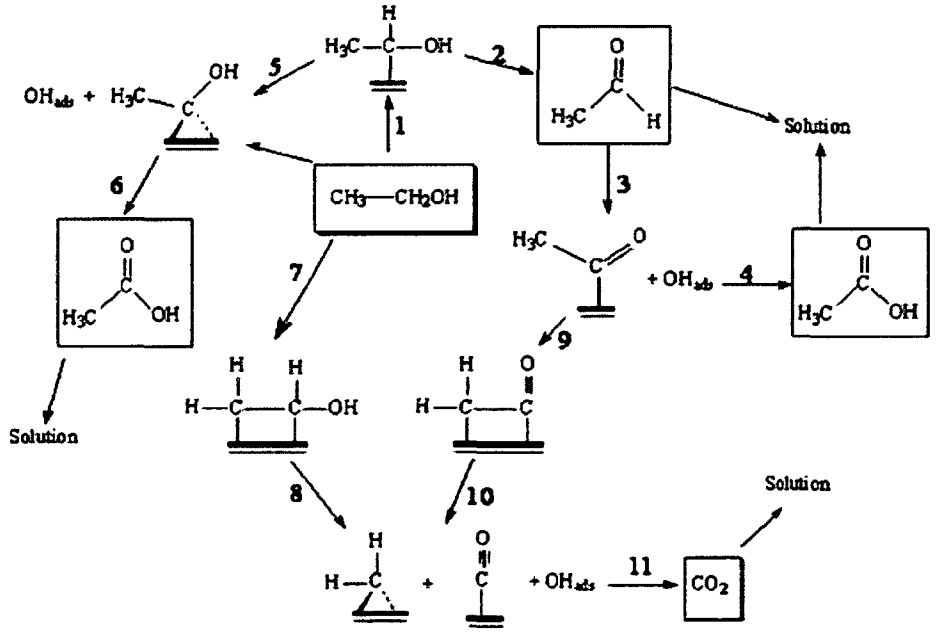

Figure 2.4:General reaction scheme for ethanol oxidation on Pt-Sn[18]

Rousseau et al.[7], have also suggested a bifunctional reaction mechanism for electrooxidation of ethanol on PtSn, explained in the following Equations 2.3-2.9. They assume CO oxidation occurs via bifunctional reaction mechanism where Sn activates water at low potentials.

$$Pt + CH_3\text{-}CH_2OH \rightarrow Pt\text{-}(OCH_2\text{-}CH_3)_{ads} + e^- + H^+ \quad (2.3)$$

Or,

$$Pt + CH_3\text{-}CH_2OH \rightarrow Pt\text{-}(CHOH\text{-}CH_3)_{ads} + e^- + H^+ \quad (2.4)$$

$$Pt\text{-}(OCH_2\text{-}CH_3)_{ads} \rightarrow Pt + CHO\text{-}CH_3 + e^- + H^+ \quad (2.5)$$

Or,

$$Pt\text{-}(CHOH\text{-}CH_3)_{ads} \rightarrow Pt + CHO\text{-}CH_3 + e^- + H^+ \quad (2.6)$$

Once acetaldehyde(AAL), $CHO\text{-}CH_3$ is formed, it can absorb onto platinum sites:

$$Pt + CHO\text{-}CH_3 \rightarrow Pt\text{-}(CO\text{-}CH_3)_{ads} + H^+ + e^- \quad (2.7)$$

As Sn is known to activate water at lower potentials than Pt, some OH species form on Sn catalyst sites at low potentials:

$$Sn + H_2O \rightarrow Sn\text{-}(OH)_{ads} + e^- + H^+ \quad (2.8)$$

Adsorbed acetaldehyde can react with the OH species to produce acetic acid(AA), $CH_3\text{-}COOH$:

$$Pt\text{-}(CO\text{-}CH_3)_{ads} + Sn\text{-}(OH)_{ads} \rightarrow Pt + Sn + CH_3\text{-}COOH \quad (2.9)$$

In this mechanism, ethanol undergoes dissociative adsorption on platinum sites through an O or C adsorption process in Equations 2.3 & 2.5 or 2.4 & 2.6, respectively. The formed acetaldehyde is adsorbed onto platinum sites(Equation

2.7) and reacts with OH species adsorbed on Sn in Equation 2.9. The ability of Sn to activate water at lower potentials, shown in Equation 2.8, is essential to the adsorption of OH.

The above mechanisms were developed with data collected using binary Pt-Sn catalysts. It is generally accepted that ruthenium plays a similar role to tin, increasing activity through allowing the bifunctional mechanism to occur at low potentials. In DMFC studies, it was shown to increase the methanol adsorption rate on platinum sites[7].

Chapter 3 : Theory of Proton Exchange Membrane (PEM) Fuel Cell and its Operation

Fuel cells are electrochemical devices that directly convert certain fuels to electricity through electrooxidation. Proton Exchange Membrane fuel cells(PEMFC) consist of two electrodes, a positively charged anode and negatively charged cathode, between which a polymer electrolyte membrane is sandwiched. The schematic of a single PEM fuel cell is shown in Figure 3.1. The outer shell of the cell, which provides a means of fastening the two sides together is provided by two aluminum alloy end plates(shown in black). Two insulating layers(shown in light blue) sit between the end plates and the copper current collector plates(shown in orange). The current collector plates are placed against poco graphite blocks(shown in gray) which have a specific flow field machined into them. The flow fields are gas flow channels, which typically have serpentine patterns. The graphite blocks conduct electrons to the copper current collecting plates, which can be connected to an external load.

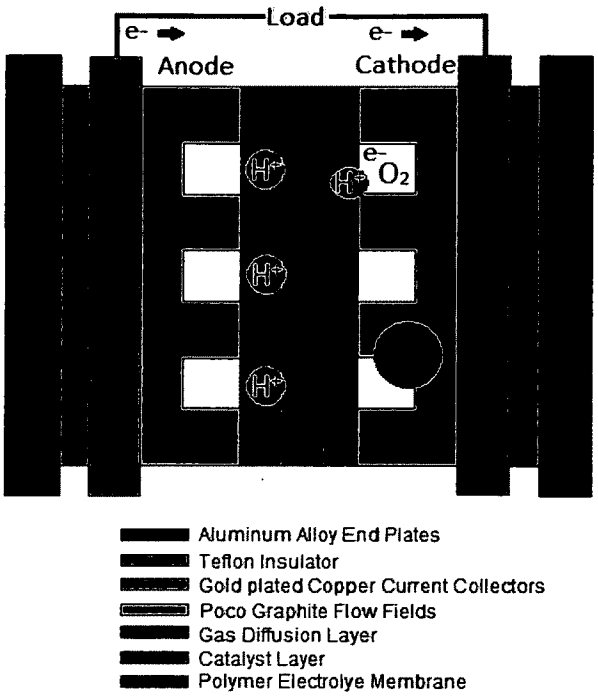

Figure 3.1: Schematic of a PEM Fuel Cell

Fuel is passed through the flow field on the anode side, while an oxidant is fed to the flow fields on the cathode side. Both anode and cathode electrodes consist of a gas diffusion layer(GDL), shown in purple, and a catalyst layer shown in green. Sandwiched between the two electrodes is a polymer electrolyte membrane shown in red. The fuel feed to the anode side is typically hydrogen or an alcohol while the oxidant supplied to the cathode side is oxygen or air. In the case of hydrogen, the gas reacts with the catalysts, dissociating it into protons and electrons, described by Equations 3.1-3.3. In the case of ethanol, the fuel is oxidized first into intermediate species and hydrogen, then the hydrogen is dissociated into protons and electrons, while the intermediates are finally oxidized to CO_2(Eq. 3.4). The protons pass through the electrolyte

membrane and react with the oxygen at the cathode catalyst to form water(Eqation 3.3/3.6). The electrons flow through the collector plates and travel through an external circuit, providing electrical power for any load connected to the fuel cell.

The half cell and overall reactions for a hydrogen PEM fuel cell are given as:

Anode: $H_2 \rightarrow 2H^+ + 2e^-$ (3.1)

Cathode: $\frac{1}{2}O_2 + 2H^+ + 2e^- \rightarrow H_2O$ (3.2)

Overall: $H_2 + \frac{1}{2}O_2 \rightarrow H_2O$ (3.3)

The half cell and overall reactions for a Direct Alcohol Fuel Cell (DAFC) are given as:

Anode: $CH_3CH_2OH + 3H_2O \rightarrow 2CO_2 + 12H^+ + 12e^-$ (3.4)

Cathode: $3O_2 + 12H^+ + 12e^- \rightarrow 6H_2O$ (3.5)

Overall Reaction: $CH_3CH_2OH + 3O_2 \rightarrow 2CO_2 + 3H_2O$ (3.6)

Under ideal conditions, the reaction given in Equation 3.3 can generate 1.23 volts. Under practical operating conditions, the actual cell voltage is normally less than 1 volt. To achieve a greater output voltage, fuel cells are connected in series to form stacks.

The basic components of a single PEMFC system are:

- A five layer membrane electrode assembly(MEA). The inner layer is a proton conducting polymer electrolyte membrane which is sandwiched

between two catalyst layers. Two gas diffusion layers(GDLs) makeup the outermost layer of the MEA.

- On each side of the MEA, graphite plates with flow field patterns provide flow channels for fuel and oxidant. The graphite plates are connected to copper current collecting plates that can be connected to an external load circuit. Aluminum alloy end plates comprise the shell of the fuel cell. The plates have threaded holes for mounting screws that secure the cell assembly. These components make up a typical single PEM fuel cell.
- Auxiliary equipment is used to monitor and control temperature, pressure, humidification and gas or liquid flow rates.

PEM type fuel cells are operated at low temperature, and are ideal for use in small electronic devices as well as automobiles. Oxidants are typically air or oxygen, and with complete oxidation, the byproducts are CO_2 and H_2O for alcohol based fuel cells. Hydrogen has an energy density of 68,000BTU per ft^3, and is easily electrooxidized in a fuel cell, with the only generated byproduct being water. Due to hydrogen cost, fuel infrastructure, and storage concerns, alcohols(methanol and ethanol) have become viable alternatives[3].

The greater complexity of ethanol leads to the difficulty in efficient electrooxidation in a fuel cell. The mechanism given by Equations 3.4-3.6 above describes the reactions occurring in a DAFC operating on ethanol. The most commonly reported intermediates, in addition to those in the provided in the mechanism, are acetaldehyde, acetic acid, and carbon monoxide. Depending on the catalysts used, these intermediates will be present in different quantities as

products due to incomplete oxidation of the each intermediate. The complexity of ethanol electrooxidation is discussed by Bergamaski et al.[4], where for ethanol a single C-C bond must be broken and three CO bonds formed(Equation 2.4 & Figure 2.4) before oxidation of carbon monoxide to CO_2 can proceed. This is in contrast with methanol where only one CO bond must be formed.

3.1 Membrane Electrode Assembly

The MEA can be considered the heart of a PEM fuel cell. It consists of three primary components; a polymer electrolyte membrane, gas diffusion layers and catalyst layers. The catalyst layers are located on either side of the membrane. The catalyst can be applied to the anode and cathode GDLs, or directly to the membrane, creating a Catalyst Coated Membrane(CCM). Preparation of the MEA is discussed later in Chapter 4.

3.2 Polymer Electrolyte Membrane(PEM)

If we consider the MEA to be the heart of a PEM fuel cell system, the polymer electrolyte membrane can be considered the heart of the MEA. The membrane allows the conduction of protons while preventing electrons from passing through. The membrane does not allow fuel or oxidant to permeate to the anode or cathode, respectively, and acts as an insulator. Fuel permeation, or crossover, is specifically important in alcohol fuel cells, where fuel crossover plays a large role in performance and efficiency.

Nafion® is the most commonly used membrane in PEM fuel cells today. Manufactured by DuPont, Nafion® was invented in the early 70's as a replacement for the previously used phenolic membranes. Compared to it's predecessor, Nafion® reduces fuel crossover, is thermally and mechanically more durable, and has approximately twice the ionic conductivity.

Nafion® has become an industry standard, against which all other developmental and commercial membranes are compared. Given it's high cost and environmental disposal hazards, researchers and competitors are constantly looking for alternatives. Nafion® is a perfluorosulfonic acid membrane. In addition to Nafion®, there are many commercially available perflorinated polymer electrolye membranes including Aciplex by Asahi Chemicals Co., Flemin by Asahi Glass Co., and PRIMEA by W.L. Gore and Associates, Inc.

The base polymer for all of the commercial membranes is polyethylene. To create a perfluorinated membrane from polyethylene the base structure is altered such that the hydrogen atoms are replaced by fluorine, creating polytetrafloroethylene(PTFE), also know by the trade name, Teflon®. The bonds between the carbon and fluorine make Teflon® highly durable, and resistant to chemical attack. It is also strongly hydrophobic, ideal for use in a fuel cell, where it can repel the generated water[1].

To create a proton conducting electrolyte from Teflon®, sulphonation of the polymer is required. This process adds a side chain ending with suphonic acid, HSO_3. Sulphonic acid is highly hydrophyllic. Combined with the hydrophobicity of Teflon®, water clusters can be formed within the membrane.

The method by which suphoniation is carried out varies with the base membrane structure but the outcome is the same. The sulphonic acid group is ionically bonded such that the end of the side chain is a SO_3- group, and an H^+ ion. The SO_3- group is strongly attached. When hydrated, the H^+ ions are weakly attracted to SO_3-, and are able to move within hydrated regions, conducting protons through an electronically resistant material.

One of the factors contributing to lack of commercial production of PEM fuel cells is cost. Nafion® currently retails for over $1000 per square meter(www.FuelCellStore.com). This makes it one of the most expensive components in a fuel cell. It represents just one of the problems with Nafion®.

3.3 Alcohol Crossover

In addition to cost, when used in alcohol fuel cells Nafion® can lead to a significant amount of fuel crossover. In direct alcohol fuel cells, ethanol concentrations above 1M result in a large drop in maximum power output due to fuel crossover[15]. With an increase in fuel concentrations and temperature, the ethanol crossover rate through Nafion® increases[25]. Crossover is the diffusion of fuel across the membrane due to the concentration gradient of ethanol between the anode and cathode. Crossover can greatly affect the performance of a direct alcohol fuel cell. In addition to reducing fuel utilization, ethanol can react with adsorbed oxygen at the cathode catalyst sites creating a mixed potential at the cathode. Further, ethanol and it's intermediate products can be

adsorbed on the cathode catalyst surface, decreasing the oxygen reduction rate[26].

Reducing crossover is an important step in the development of viable DAFC systems. In general, Nafion® -115 is used in direct ethanol fuel cells. Nafion® membranes are characterized by there equivalent weight(EW) and thickness. Nafion® 115 has an EW of 1100 and a thickness of 0.005inches[27]. The EW is the weight of Nafion per mole of sulfonic acid group. Thinner membranes are known to have higher proton conductivity[28]. In a DAFC, thinner membranes are less ideal, as they are prone to greater fuel crossover versus a thicker one. A thickness too great will impede conductivity, so for DAFC systems, Nafion® 115 is chosen[15, 25, 29, 30].

For direct methanol fuel cells(DMFCs), multiple alternatives to Nafion have been studied including polyether ketone[31], polyvynil alcohol[32], acid doped polybenzimidazole[33] and polyphosphazene[34]. These offer the benefit of being low cost and environmentally friendly. At present, Nafion® is the primary focus of research for DAFC systems. As more research is directed toward DAFCs, the membrane is one area in need of investigation for ethanol based fuel cells.

A high operating temperature is typically associated with greater performance in PEM fuel cells. One limitation to Nafion® is that the conductivity is highly dependent on hydration. This requires temperatures be lower than 100°C. Given the slow and complex reaction kinetics of ethanol electrooxidation, higher temperatures are favored, which is further evidence of the need for a more

specialized membrane. Higher operating temperatures have also been shown to increase ethanol crossover through Nafion®. This can be attributed both to the properties of Nafion® at high temperatures, and to the accelerated thermodynamic motion of ethanol at high temperatures, both facilitate the transport of ethanol through the membrane.

Currently, researchers have only begun to understand the behavior of ethanol crossover through Nafion®. While this study does not focus on the membrane, it is necessary to understand the limitations pertaining to the materials being used. It is possible, through optimized gas diffusion layers, flow fields and a highly specialized catalyst, ethanol utilization can be increased enough to offset the crossover limitations of Nafion®.

3.4 Gas Diffusion Layer(GDL)

The GDL is considered one of the most important parts of the membrane electrode assembly. The gas diffusion layer is typically made of a porous carbon paper or fabric. Carbon is chosen due to its relatively low cost and high electrical conductivity. The GDL serves multiple purposes. In addition to providing a conducting path for electrons between the catalyst layer and current collecting plates, the GDL aids in diffusion of reactants to catalyst sites, as well as in water management.

Typically, GDLs are between 100-400um thick. Thinner GDLs are typically more desirable as they provide a minimum electrical resistance while offering a shorter diffusional path for reactant and product fluids[1]. GDLs are

generally wet proofed with a material like Teflon®. A hydrophobic material is necessary to prevent the GDL from absorbing water and to reject water from the cell. Water removal prevents flooding, a condition when excess water is present in the GDL layer, preventing fuel or oxidant from reaching the catalyst layer. Flooding drastically reduces cell performance. While preventing flooding is desired, the membrane requires hydration to conduct protons. The GDLs wet proofing needs to allow the proper amount of water to reach the membrane and repel any excess. For optimum water management, a minimum amount of PTFE content, combined with a thin gas diffusion layer with large pores is suggested[35, 36]. Reduced thickness is important, but too thin will increase the potential for fuel crossover. Pore sizes have been studied, and Prasanna et al.[37] found that pores larger than 40nm can lead to flooding.

Several types of GDLs are commercially available for PEM fuel cells. Of the fabric GDLs, one of the most common is ELAT, manufcatured by Etek. The most commonly used carbon paper GDL is Toray. It provides very high performance and has established itself as an industry standard. The differences in the types of GDLs has been studied by Moreira et al. [38], where it was found that paper GDLs offer better performance at low current densities, while fabric offers superior water management and is better suited for high current densities.

The most important advancement to gas diffusion layers is microporous layer(MPL). The MPL is a porous, hydrophobic layer typically consisting of PTFE and carbon[39, 40]. The MPL improves water management in the GDL. The optimum PTFE content in the MPL is reported as a wide range between 20-45%

[37, 40, 41]. The actual optimum PTFE content in the MPL will depend on the GDL substrate properties and wet proofing. The MPLs can also help with the evolution of product gasses in the case of CO_2 formation at the anode of alcohol fuel cells by providing micropores for gas removal[31, 42, 43].

In a DAFC the fuel is a solution of ethanol and water, hence GDLs with enhanced water management properties are highly sought after. Previous work at the University of New Hampshire successfully studied the role of GDLs and MPLs with various hydrophobicity in DMFCs[2]. The study successfully optimized the MPL to achieve peak power output of 150mW/cm^2. The same optimization of MPLs for ethanol based fuel cells has yet to be developed.

3.5 Catalyst Layer

The catalyst layer, also known as the active layer, is located between the GDL and membrane as shown in Figure 3.1. The search for effective catalysts for DAFCs is the subject matter of this investigation. Some work is reported in the literature review to be found in Chapter 2. The catalyst layer can be placed on the GDL, creating a gas diffusion electrode(GDE) or on the surface of the membrane, creating a catalyst coated membrane(CCM). The purpose of the catalyst layer is to accelerate the reaction kinetics of the anode and cathode reactions. At the anode, the ethanol oxidation reaction(EOR) takes place, and with complete oxidation, the products are CO_2 and H_2O. At the cathode, the oxidation reduction reaction(ORR) takes place. In a hydrogen fueled PEM fuel cell, the reaction kinetics at the cathode are slow compared to the reduction

reaction of hydrogen at the anode. This is reversed for alcohol fuel cells, where the oxidation of ethanol is a multi-step process, and is considerably slower than the ORR.

The mechanism for electrooxidation of ethanol is given by Equations 3.4-3.6. The mechanism assumes complete electrooxidation of ethanol. In reality, the reaction produces several intermediates which are not easily oxidized. Those intermediates are acetic acid and acetaldehyde. These also act as poisons, occupying active catalyst sites, preventing the uptake of ethanol.

Catalyst requirements are measured on the basis of loadings, typically based on the amount of Pt present and reported in mg-cm^{-2}. Current DAFC studies report Pt loadings of anode catalysts for the EOR in the range of 1-4mg-cm^{-2}[7, 15, 29, 30, 44]. The optimal catalyst loading for ethanol electrooxidation is not yet known. Low loadings cause low performance due to inadequate number of active sites available for the ethanol uptake, while too high a loading can cause blockages in the pores of the gas diffusion layer, or increased internal resistance due to the thickness of the layer.

Typically for DAFCs, the electrocatalyst is a bimetallic Platinum-Tin supported on XC-72 Carbon. Carbon supports provide a large active surface area for catalyst dispersion. To optimize catalyst loading, multiple catalyst deposition techniques as well as improved supports have been studied. Typically in research, catalysts are prepared in a slurry and hand-painted onto GDL surfaces. More advanced techiques include the preparation of CCMs, in which catalyst is applied directly to the membrane via a spray or decal printing

method. Studies have shown these methods can offer the same catalyst loadings as painting, while increasing the utilization of the catalyst[45]. Another method for CCM preparation is chemical vapor deposition, in which a pure metal is deposited directly to a target surface, in most cases a GDL or membrane. While an expensive method, and one that doesn't allow for high metal loadings, it has proven to produce a more efficient catalyst layer[46].

3.6 Water Management & Crossover Effects

The hydration of the proton conducting membrane is a critical function for proper fuel cell operation. Maintaining and controlling the hydration of the membrane is known as water management. The membrane must be properly saturated with water to allow proper proton conductivity, while at the same time the amount of water must also be limited so as not to allow flooding of the GDLs which causes mass transport impedance. Some of the more major factors contributing to water transport are water drag through the cell, back diffusion from the cathode and diffusion of any water in the fuel stream through the anode. Water drag is caused by electro-osmotic drag, which is the action of water molecules carried through the membrane with protons[47]. Each proton can pull with it between 1 and 5 water molecules[1]. The drag increases with current densities, meaning that at high power draw the anode can dry out. Back diffusion is the flow of water from the cathode to anode due to pressure and concentration gradients.

In PEM fuel cells operating temperatures are typically maintained at 60°C and above, as they facilitate increased reaction kinetics. At these temperatures, dry fuel and oxidant gases dry out the electrodes faster than water is produced. To combat the drying of the cell, the fuel and oxidant streams are humidified. The actual amount of humidification required is unique to specific operating conditions.

While humidification greatly improves cell performance, the addition of complex humidification and water recovery systems is costly. One scientific advance has been self humidifying membranes. These are membranes with additional catalyst applied around the perimeter of the catalyst layer, or integrated into the membrane itself. The addition of the catalyst allows the membrane to oxidize H_2 lost to crossover, forming H_2O and maintaining water equilibrium[48]. While H_2 crossover in a PEM doesn't seem possible, in industry it is understood that hydrogen crossover can occur at certain conditions during shutdown and startup of a fuel cell.

In DAFCs, water management is critical. Present research has not yet discovered a way to prevent the crossover of fuel from the anode to cathode. In addition, the two-phase flow of gaseous products and liquid intermediates and fuel at the anode must dealt with. Simultaneous effluent gas and water removal could be facilitated by micro porous layers(MPLs) applied to GDLs, or the use of a modified flow field. Work at UNH has demonstrated that MPLs can build up hydraulic pressure and limit water transport through the membrane[2]. At

present, work is being done to characterize ethanol crossover in DAFCs, but nothing has been achieved by way of reduction or prevention[44].

3.7 Theoretical Open Circuit Voltage

Based on equations 3.1-3.3, the overall electrochemical reaction in a hydrogen fueled PEM fuel cell is the same as the combustion reaction for hydrogen in air. The standard reversible potential, or open circuit voltage, E^o, can be determined by equation 3.7,

$$E^o = \frac{-\Delta G^o}{nF} \qquad (3.7)$$

where ΔG^o, n and F are the change in Gibbs free energy, the number of electrons present(2 in the case of H_2), and Faraday's constant, 96,485 Coulombs/mol, respectively.

The change in Gibbs free energy, ΔG^o, is the amount of energy that can be produced and is defined by equation 2.8,

$$\Delta G^o = \Delta H - T \cdot \Delta S, \qquad (3.8)$$

where ΔH, T, and ΔS are the change in enthalpy, the temperature in Kelvin, and the change in entropy, respectively. At 25°C, ΔH for hydrogen is 286kJ/mol, and the change in entropy is 0.163 kJ/mol. Substituting these values in Equation 3.8, the Gibbs free energy for hydrogen is approximately 237kJ/mol. The open circuit voltage can then be calculated by Equation 3.7 to be 1.23v.

Equations 3.7 and 3.8 can also be applied to the overall reactions for the electrooxidation of ethanol given by Equations 3.4-3.6. The Gibbs free energy is determined to be 1,325.7kJ/mol, and the open circuit voltage is 1.145v.

The theoretical maximum efficiency of a fuel cell is another way to evaluate and compare different fuels. Efficiency is defined as the ratio of useful energy output to energy input. In the case of a fuel cell, the electrical energy produced is the output, and the energy input as the enthalpy of the fuel[27]. Assuming all of the Gibbs free energy is converted to electrical energy, the efficiency, η, is:

$$\eta = \frac{\Delta G}{\Delta H} \qquad (3.10)$$

where ΔH, and ΔG are the change in enthalpy and Gibbs free energy in kJ/mol, respectively. For a hydrogen fuel cell the maximum theoretical efficiency determined through equations 3.8 and 3.10 is 83%. The same equations can be applied to ethanol. Given that the enthalpy of combustion of ethanol is -1370kJ/mol, the maximum theoretical efficiency of a direct ethanol fuel cell is 96.7% .

Given that a fuel cell is rarely operated at standard conditions, the Nernst equation, provided as equation 3.11, describes the theoretical potential, E_t for all conditions.

$$E_t = E^o - \frac{RT}{zF} \ln\left(\pi_i a_i^{v_i}\right) \qquad (3.11)$$

In Equation 3.11, E^o is the open circuit voltage in volts, R is the gas constant in J K^{-1} mol^{-1}, T is the temperature in Kelvin, F is Faraday's constant (96,485 Coulombs/mol), z is the number of moles of electrons transferred, a_i is the activity of species i, v_i is the stoichiometric coefficient of species i, and π is the product. In the case of a hydrogen fueled PEM fuel cell, assuming the gases are ideal, the activities of the gases are equal to their partial pressure, P at 1atm, and the activity of water is equal to 1. Therefore, the theoretical voltage, E_t, can be expressed as,

$$E_t = E^o - \frac{RT}{zF}\ln\left(\frac{1}{P_{H_2}(0.21P_{air})^{1/2}}\right) \qquad (3.12)$$

where E^o is the open circuit voltage in volts, R is the gas constant in J K^{-1} mol^{-1}, T is the temperature in Kelvin, F is Faraday's constant (96485 Coulombs/mol), z is the number of moles of electrons transferred, P_{H2} is the partial pressure of hydrogen and P_{aur} *is* the partial pressure of air. This can be thought of as an irreversible voltage. At standard conditions, the value is 1.219V, a loss of 0.011V from the reversible, ideal open circuit voltage. In general, the actual open circuit voltage will be less than the theoretical value. As more current is drawn, voltage produced from the cell decreases.

3.8 Overpotentials

With increasing electrical load, or current draw on a fuel cell, the operating voltage drops. Current density vs potential curves, also known as Polarization curves provide a graphical representation of voltage drop in a fuel cell relative to

current density. The polarization curve in Figure 3.2 is an example of a typical hydrogen fueled PEM fuel cell.

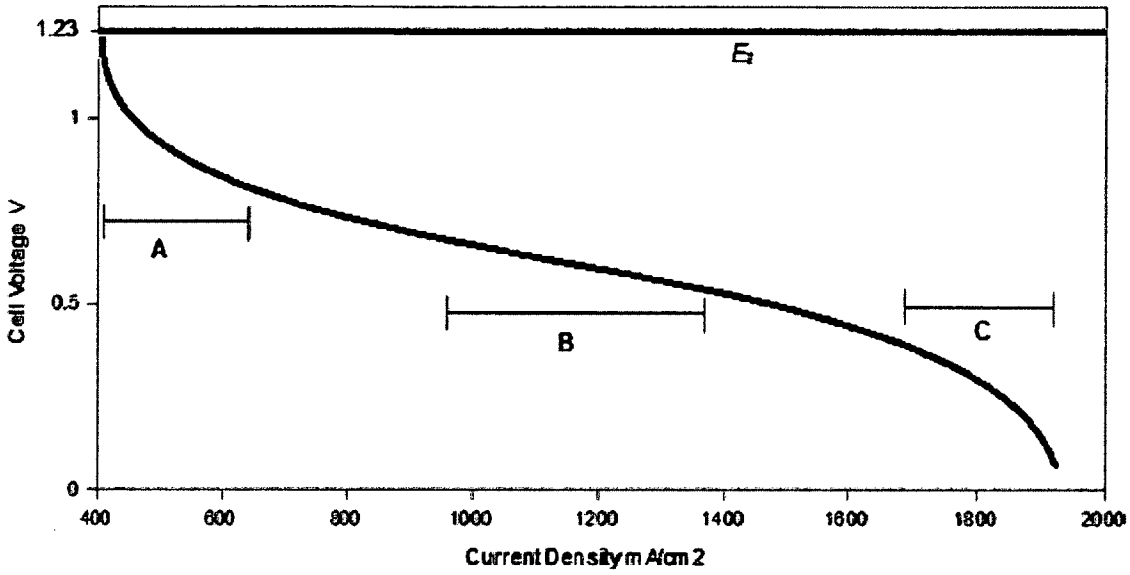

Figure 3.2: Example of fuel cell overpotentials

The lower, black line represents actual performance, while the upper dark blue line represents the ideal, theoretical open circuit voltage, E_t. The differences in the curves are due to three irreversible voltage losses; Activation Overpotential (A), Ohmic Overpotential (B) and Concentration, or Mass Transport Overpotential(C).

3.8.1 Activation Overpotential

At low current densities, activation losses, "A" dominate the polarization curve due to electrode kinetics. A certain amount of potential is required to start the electrochemical reaction which is determined by the activation energy for the

reaction. The losses occur at both the anode and cathode and can be determined by the Butler-Volmer equation. The voltage loss, $\Delta V_{act,c}z$, due to activation overpotential at the cathode is defined by the difference between the reference voltage, $E_{r,c}$, and the actual voltage, E_c as given in equation 3.13.

$$\Delta V_{act,c} = E_{r,c} - E_c \qquad (3.13)$$

A similar expression is also given for the anode, $\Delta V_{act,a}$, in equation 3.14,

$$\Delta V_{act,a} = E_a - E_{r,a} \qquad (3.14)$$

where E_a and $E_{r,a}$ are the anode voltage and reference anode reference voltage, respectively. The cathode overpotential is determined by equation 3.15 below,

$$\Delta V_{act,c} = \frac{RT}{\alpha_c F} \ln\left(\frac{i}{i_{0,c}}\right) \qquad (3.15)$$

where R, T, F, α_c, i and $i_{0,c}$ are the universal gas constant, the temperature in Kelvin, Faraday's constant, the cathodic charge transfer coefficient, the current density and the cathode reaction exchange current density, respectively. A similar expression is used to determine the anode activation overpotential and is given by equation 3.16.

$$\Delta V_{act,c} = \frac{RT}{\alpha_a F} \ln\left(\frac{i}{i_{0,a}}\right) \qquad (3.16)$$

where R, T, F, α_a, i and $i_{0,a}$ are the universal gas constant, the temperature in Kelvin, Faraday's constant, the anodic charge transfer coefficient, the current density and the anode reaction exchange current density, respectively. The

activation overpotential, ΔV_{act}, can be simplified and determined using the Tafel equation:

$$\Delta V_{act} = A + B\ln(i) \qquad (3.17)$$

The paramaters, *A* and *B* are given by,

$$A = \frac{-RT}{\alpha F}\ln(i_0),\ B = \frac{RT}{\alpha F} \qquad (3.18\ a,b)$$

where *R*, *T*, *F*, α and i_0 are the universal gas constant, the temperature in Kelvin, Faraday's constant, the charge transfer coefficient, and the exchange current density, respectively. The term ΔV_{act} in equation 3.17 is the difference between the cell voltage and reference as given in equations 3.13 and 3.14 for the cathode and anode, respectively. The cell voltage, E_{cell} is determined by the difference between the reference voltage(theoretical cell potential, E_r) and anode and cathode voltage losses. Combining the expressions yields equation 3.19,

$$E_{cell} = E_r - \frac{RT}{\alpha_c F}\ln\left(\frac{i}{i_{0,c}}\right) - \frac{RT}{\alpha_a F}\ln\left(\frac{i}{i_{0,a}}\right) \qquad (3.19)$$

where *R*, *T*, *F*, α_c, α_a, $i_{0,c}$ and $i_{0,a}$ are the universal gas constant, the temperature in Kelvin, Faraday's constant, the cathode charge transfer coefficient, anodic charge transfer coefficient, the cathode exchange current density and the anode exchange current density, respectively. Due to the higher rate of the anode reaction kinetics, the anode exchange current density, $i_{0,a}$, is significantly greater than that of the cathode. The activation overpotential of the anode can then be removed from equation 3.19, and the equation becomes.

$$E_{cell} = E_r - \frac{RT}{\alpha_c F} \ln\left(\frac{i}{i_{0,c}}\right) \qquad (3.20)$$

Equation 3.20 shares the same form as the Tafel equation. Equation 3.20 implies that the cathode exchange current density has the maximum influence on activation overpotential. This is due to the signifcantly slower reaction kinetics of the cathode oxygen reduction reaction(ORR) vs the hydrogen oxidation reaction(HOR).

3.8.2 Ohmic Overpotential

Ohmic losses are those that occur due to resistance to the flow of ions through the system. These losses can be ionic due to the MEA, electronic resistance, or contact resistance. The losses typically cause a linear voltage drop throughout the middle of the polarization curve, shown in Figure 3.2 as the region labeled "B". The overpotential ΔV_{ohm}, is determined by Ohm's law,

$$\Delta V_{ohm} = iR_i \qquad (3.21)$$

where i and R_i are the current density in A/cm^2 and total internal resistance of the cell in ohms-cm^2. The total resistance can be determined by equation 3.22,

$$R_i = R_{i,i} + R_{i,e} + R_{i,c} \qquad (3.22)$$

where $R_{i,i}$, $R_{i,e}$, and $R_{i,c}$ are the ionic, electronic and contact resistances in Ωcm^2, respectively. In general, electronic resistances are almost negligible. The typical values for R_i are in the range of 0.1-0.2Ωcm^2[27].

3.8.3 Concentration Overpotential

At high current densities, reactants are consumed quickly at the electrode, faster than the rate of diffusion, which causes a concentration gradient. When hydrogen and oxygen are used the concentration gradients are low, as their rates of diffusion are high. Therefore, the concentration overpotential, ΔV_{conc}, is small. Still, the formation of water at the cathode can impede the diffusion through the GDL, causing concentration gradients and mass transport losses. The Nernst equation describes the concentration profile in equation 3.23.

$$\Delta V_{conc} = \frac{RT}{zF} \ln\left(\frac{C_B}{C_S}\right) \qquad (3.23)$$

where R is the gas constant in J K^{-1} mol^{-1}, T is the temperature in Kelvin, F is Faraday's constant (96485 Coulombs/mol), z is the number of moles of electrons transferred, and C_B and C_S are the bulk concentration of the reactant and the concentration of the reactant at the catalyst surface in mol cm^{-3}, respectively. Manipulation of Ficks law through the steady state approximation tells that the rate of reactant consumption is equal to the diffusional flux allows the concentration gradient to be directly related to the current, i, below:

$$i = \frac{zF \cdot D \cdot (C_B - C_S)}{\delta} \qquad (3.24)$$

where z is the number of moles of electrons transferred, F is Faraday's constant(96,485 Coulombs/mol), D is he diffusion coeffient of the reacting species in cm^2 s^{-1}, δ is the diffusion distance in cm, and C_B and C_S are the bulk

concentration of the reactant and the concentration of the reactant at the catalyst surface in mol cm^{-3}, respectively. The concentration of reactant at the catalyst surface is current density dependent. At high current densities the surface concentration is low, since more reactant is consumed. The current density at which reactant is consumed faster than it can reach the catalyst surface is the limiting current density, i_L. The limiting current density is given by equation 3.25:

$$i_L = \frac{zFDC_B}{\delta} \qquad (3.25)$$

Rearrangement of equation 3.25 and combining it with equations 3.24 and 3.23 allows for a relationship between the concentration overpotential, ΔV_{conc}, and limiting current, i_L, density as:

$$\Delta V_{conc} = \frac{RT}{zF} \ln\left(\frac{i_L}{i_L - i}\right) \qquad (3.26)$$

where R is the gas constant in J K^{-1} mol^{-1}, T is the temperature in Kelvin, F is Faraday's constant (96485 Coulombs/mol), and z is the number of moles of electrons transferred, Equation 3.26 implies that as the limiting current is approached, the cell output will see a sharp drop in potential. Nonuniformities of the electrodes prevent cells from reaching the limiting current density in actual operation. Most likely certain areas will reach the limiting current density before others.

In addition to concentration gradient related voltage losses, fuel crossover has a major impact on the performance of direct alcohol fuel cells. Fuel crossover reduces the cells potential by the transport of fuel from the anode to

the cathode prior to oxidation. The fuel occupies active catalyst sites at the cathode where it is oxidized, causing a mixed potential. Overall, this reduces the cells potential, as the fuel is unrecoverable.

Chapter 4 : Experimental Apparatus and Procedure

The PEM fuel cell system used in this study consists of a single, 5cm^2 fuel cell, temperature, humidity and mass flow controllers, pressure gauges, electronic DC load, power supply, and computer with data acquisition hardware and software. For MEA preparation, vacuum oven, hot press and hot plate with magnetic stirrer were used. Catalyst synthesis required a condenser column and heating mantle.

4.1 Fuel Cell System

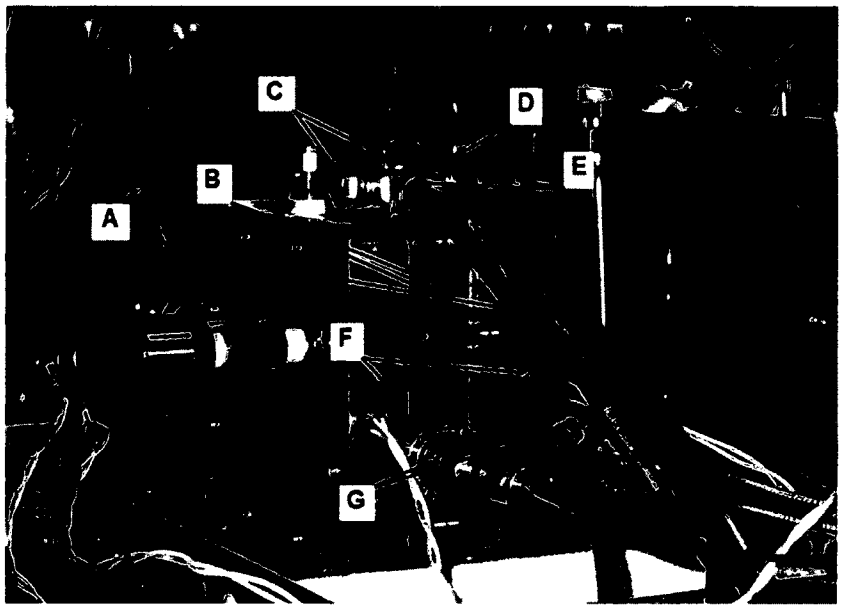

A) Aluminum Alloy End Plates
B) Poco Graphite Blocks
C) Gold Plated Current Collector Plates
D) Thermocouples
E) Power Leads
F) Cartridge Heaters
G) Quick Connect Gas/Liquid Outlet Lines

Figure 4.1: External Fuel Cell Components

The fuel cell hardware consists of a pair of 3x3" Poco Graphite grade AXF-5Q blocks shown in Figures 4.1 and 4.2 as B and A, respectively. Poco is used due to it's excellent electrical conductivity. The blocks have a serpentine flow-pattern machined at their centers in a $5cm^2$ square, shown in Figure 4.2 as B, which delivers fuel to the electrodes. The blocks also function as current collectors. Attached to the outside of the blocks are gold plated copper current collectors pictured in Figures 4.1 and 4.2 as C and E, respectively. The current collectors provide terminal connectors, shown as E in Figure 4.1, for high current power leads.

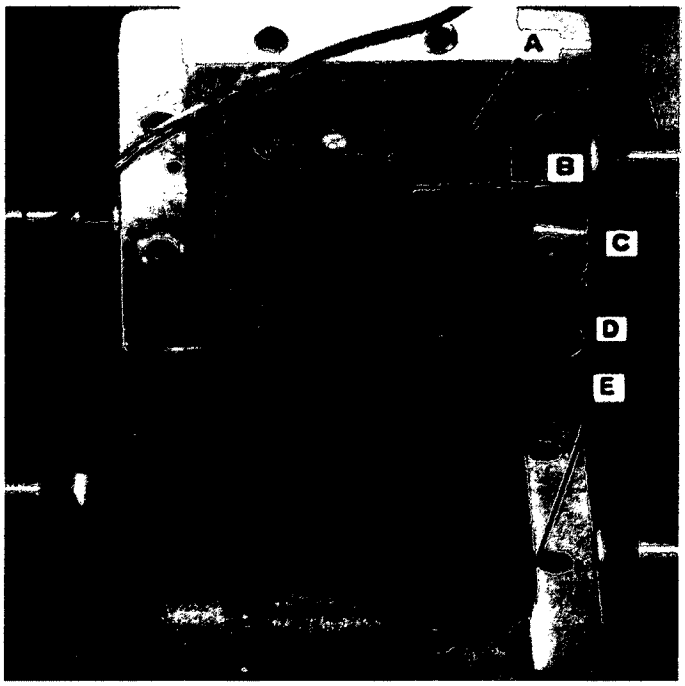

A) Poco Graphite Block
B) Serpentine Flow Field
C) Aluminum End Plate
D) Silicon Gasket
E) Gold Plated Current Collector Plate

Figure 4.2: Internal Fuel Cell Components.

Aluminum alloy end plates comprise the shell of the cell pictured in Figures 4.1 and 4.2 as A and C, respectively. The end plates hold the cell together through the use of 8 bolts arranged in an octagonal pattern. Swagelok® quick connect fittings, pictured in Figure 4.1 as G, are also mounted to the end plates which provide a secure and convenient connection system for inlet and outlet lines. A thin layer of Teflon® tape between the end plates and current collecting plates provides electrical insulation between the two layers. The end plates also have cylindrical holes machined for cartridge heaters, as well as a top mount for a thermocouple to maintain and monitor cell temperature, shown in Figure 4.1 as G and D, respectively.

4.1.1 Humidification and Temperature systems

Humidification for the gases is provided by two 12" tall, 2" in diameter stainless steel bottles and four 4" tall, 2" diameter refilling bottles full of DI water, one set for both anode and cathode. The larger bottles, labeled in Figure 4.3 by blue diamonds, are each monitored by thermocouples and wrapped with heating tape. Their temperature is maintained via PID loops in a custom LabView® program.

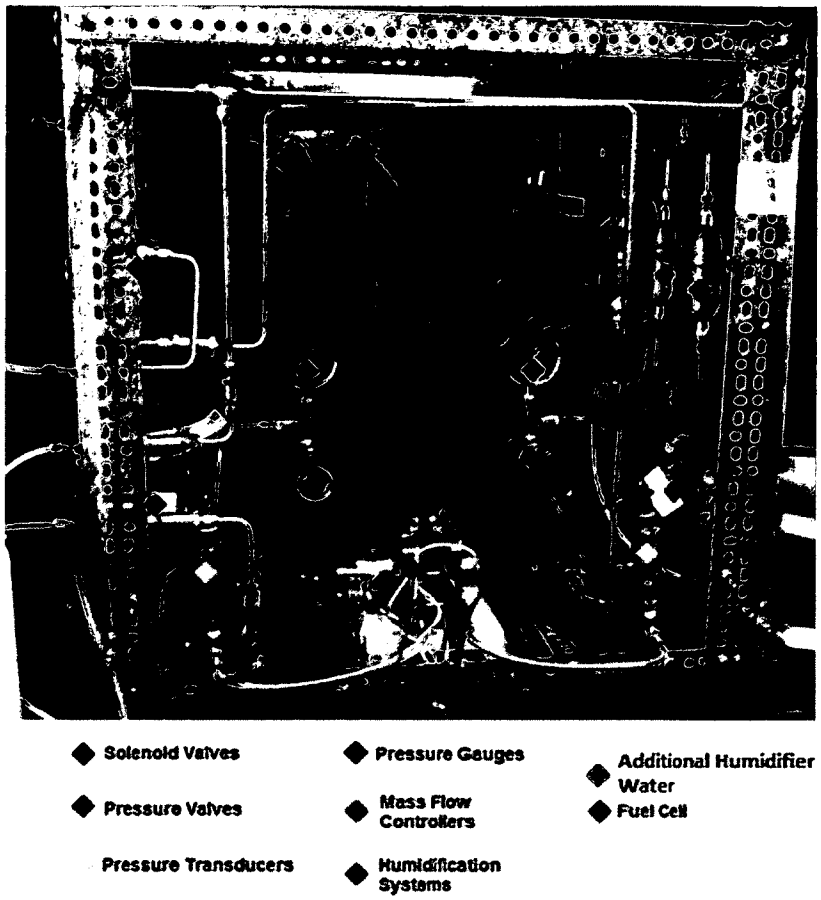

Figure 4.3: Assembled Fuel Cell System

Gas is bubbled through the large bottles to ensure saturation. The smaller bottles(pink diamonds) exist to provide additional water volume. A switch at the front of the test station opens two solenoid valves which close the humidification system to the cell and allow the operator to view the water level through two sight tubes. The levels can be checked during operation, but may cause a slight skip in performance as it bypasses gas flow around the humidification system.

Temperature to the cell is controlled by a combination of two cartridge heaters and a J type thermocouple. Like the humidifying bottles, the cell

temperature is controlled through software with a PID loop in a custom LabVIEW® program.

4.1.2 Mass Flow Controllers

Gas flow control is maintained by two Omega FMA 5400/5500 mass flow controllers, labeled with green diamonds in Figure 4.3. The hydrogen and oxygen controllers are calibrated for flows up to 1000mL/min and 2000mL/min, respectively. LabVIEW® integration of the controllers allows the operator to input desired flow rates through software and have them instantly applied.

4.1.3 Pressure gauges

Two Tescom pressure gauges, rated for 0-100psi are installed at both the anode and cathode outlet and shown in Figure 4.3 with black diamonds. Pressure valves, labeled in Figure 4.3 by orange diamonds, allow for manual application of backpressure to either side of the fuel cell. Two pressure transducers(labeled with yellow diamonds in Figure 4.3) are also present, and are intended to allow for pressure monitoring through LabVIEW®. Currently their control has not been integrated into the software, and their implementation is recommended for robust control and automation.

4.1.4 Syringe Pump

For liquid fueled systems a syringe pump provides consistent and reliable flow. A New Era NE-500 programmable syringe pump is used in all DAFC tests. The pump is controlled through proprietary software, allowing for flow rates

ranging from 0.73μL/hr to 2100ml/hr. A 60mL glass syringe is used, and must be manually refilled, or swapped for a full syringe during operation.

4.1.5 Fuel Cell System Schematic

A schematic of the fuel cell system is provided in Figure 4.4. Solenoid valves, S1-S11 control gas flow from pressurized cylinders and are-fail safe to close if system power is compromised. The system has 4 inlets, two oxidant inlets for air and O2, an inlet for N2, and an inlet for H2. Gases enter through the specified inlets and first pass through 50 micron filters(F1, F2, F3). In the case of fuel and oxidant, mass flow is controlled by the two mass flow controllers, MFC1 and MFC2, while Nitrogen gas flow is regulated manually at the tank. Each gas line has a check valve(CV1, CV2, CV3) to prevent backflow. By default, solenoid valves S2 and S3 are open to the Nitrogen lines so that the system can be purged when not in use. When engaged, the valves allow oxidant and hydrogen to pass to the humidification bypass valves, S4 and S5 for the oxidant, and S6 and S7 for hydrogen. Engaging valves S4-S7 flow oxidant and hydrogen through the humidification system, after which they enter the cathode and anode of the fuel cell, respectively. Effluent gasses leave the cathode and anode and pass by the Pressure Transducers, PT1 and PT2, and through the pressure gauges, PG1 and PG2 before exiting the system.

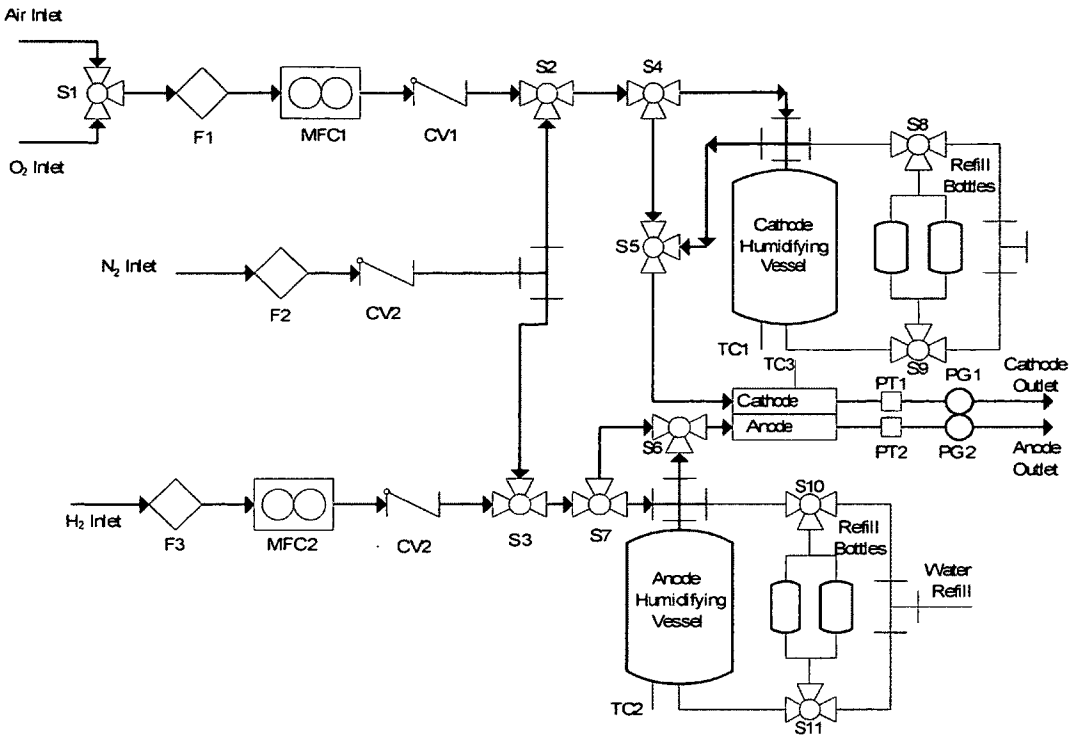

Figure 4.4: Fuel Cell System Schematic

4.2 Data Acquisition Software

All of the system components shown in Figure 4.4 are controlled and monitored through a custom LabVIEW* program. The user interface for the program is shown in Figure 4.5. Section A hosts the stop button and manual heater controls. The stop button will end the program and turn off all active switches. The Hydrogen and Oxygen switch control the heating tape on the humidification vessels, and the Fuel Cell switch controls the cartridge heaters. The three heaters can be manually controlled via their individual switches, or automatically by engaging the PID Control switch in section B of Figure 4.5.

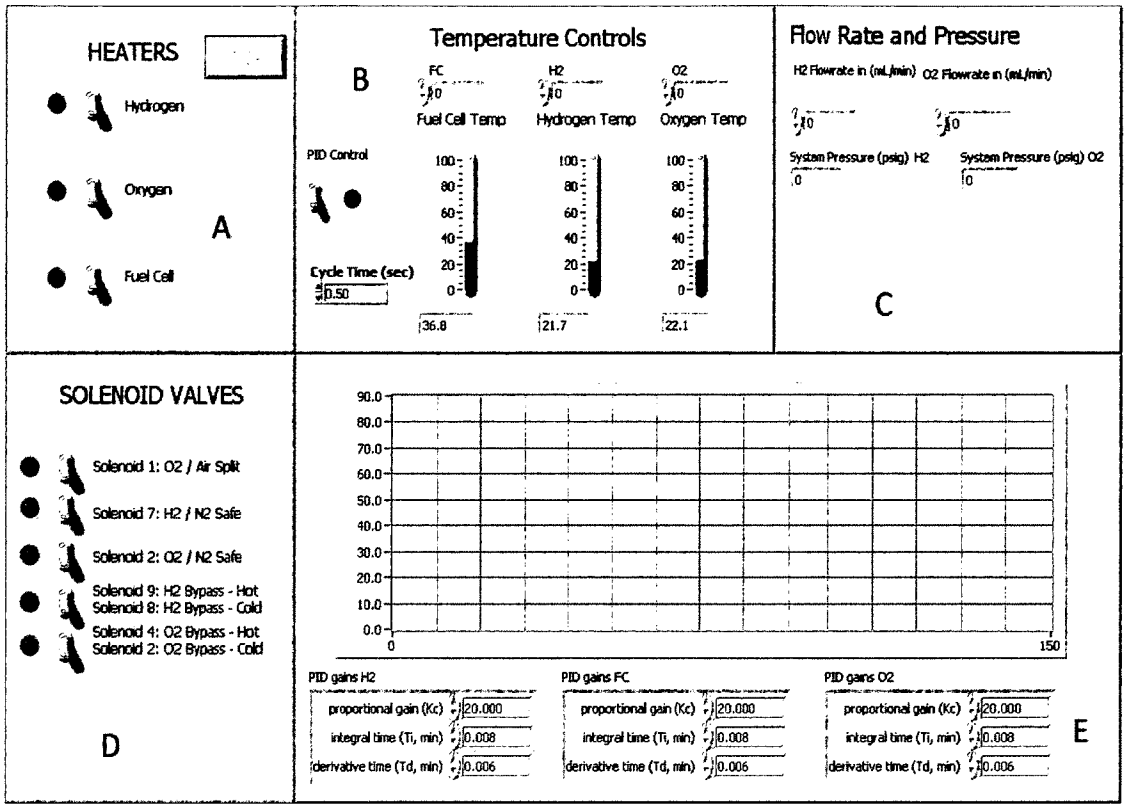

Figure 4.5: LabVIEW Fuel Cell Interface

The top three input boxes in Section B are for manual entry of set point temperatures for the fuel cell and humidifiers. Fuel Cell Temp, Hydrogen Temp, and Oxygen Temp refer to the temperature of the fuel cell, hydrogen humidifier and oxidant gas humidifier, respectively. The animated thermometers and indicators below them provide the operator with real-time measurement of the three system thermocouples, represented as TC1-TC3 in Figure 4.3 . The PID Control switch in this section engages or disengages PID(propogation, integration, derivation) loop control of the heaters. When off, the software ignores the set point temperatures and the heaters can be manually controlled

using the switches in Section A. When active, the PID loop maintains system temperatures with a 2°C tolerance.

Section C is for flow rate control and pressure monitoring. The top two entry fields allow manual input of desired flow rates in mL/min. The O_2 mass flow controller is calibrated specifically for oxygen, but will adjust the flow rate for air when the switch for Solenoid 1: O2/Air Split in Section D is engaged. The lower two boxes provide measurement of the backpressure through the Pressure Transducers, though proper integration should be completed in future studies.

Section D provides control for the 11 solenoid valves throughout the system. As discussed, the switch for Solenoid 1 controls solenoid S1 in Figure 4.3 and adjust the mass flow controller for the case when air is used as the oxidant. The switch for Solenoid 7 controls solenoid S3 in Figure 4.3. When engaged the switch opens the valve to the hydrogen inlet, and when closed allows for inert nitrogen to pass through the system. The switch for Solenoid 2 controls solenoid S2 in Figure 4.3, and like the previous switch, when off it defaults open for nitrogen purge flow. When engaged this switch allows for oxidant to enter the system. The fourth switch controls solenoid valves S4 and S5 in Figure 4.3. When engaged the switch directs hydrogen into the humidification system, and when off acts as a humidification bypass. The final switch controls solenoids S6 and S7 in Figure 4.3. When engaged the solenoids direct oxidant through the humidification system, and when off humidification is bypassed.

The controls in Section E provide direct access to the PID loop parameters through the 3 sets of 3 input boxes at the bottom of this section. The box above provides a graphical readout of the three system temperatures vs time. This allows for direct monitoring of temperature trends intended to assist the operator with diagnosis of any temperature related problems.

The NE-500 Syringe pump is controlled through software with the Windows program WinPumpTerm. The user interface for the program is shown in Figure 4.6. The desired flow rate is entered in the 'Pumping Rate' field, various units of flow can be chosen.

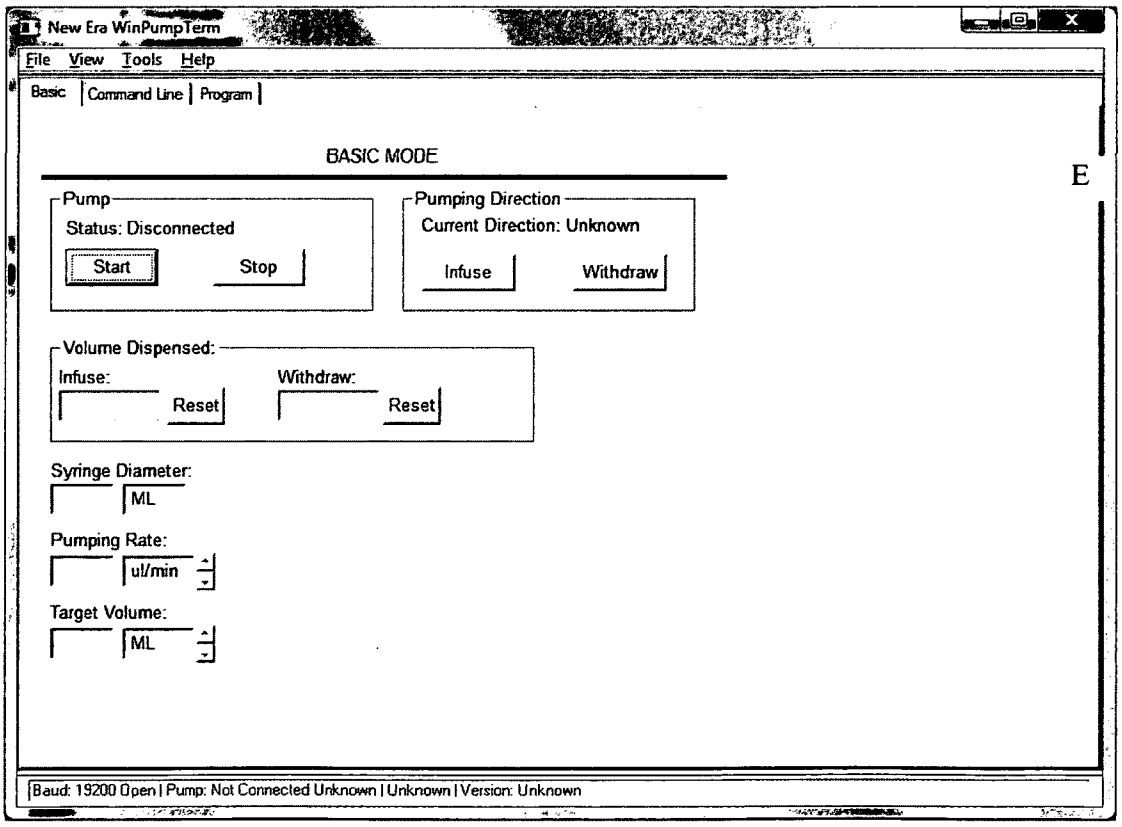

Figure 4.6: Syringe Pump Software Control Interface

4.3 Catalyst Preparation Equipment and Materials

The preparation of catalysts requires clean equipment and instruments for accurate measurements. The primary process for catalyst synthesis was through co-reduction of mixed Ions developed by [6]. The materials and procedure for the synthesis are given below.

4.3.1 Co-reduction of Mixed Ions procedure

The materials and equipment required for catalyst synthesis by Co-reduction include:

-Round bottom flask

-Condenser column

-Heating mantle

-Ethylene Glycol

-DI Water

-Plastic sample trays

-Whatman 0.2um Nylon membrane filters

-Filtration glassware, including water trap

-Vacuum pump

-Vacuum Oven

-Nitrogen

Depending on the desired catalyst, specific precursor is required. For samples prepared using Co-reduction, Chlorplatinic Acid(H_2PtCl_6) is the Platinum source, Ruthenium Chloride($RuCl_3$) is the Ruthenium source, and Tin

Chloride($SnCl_2$) is the tin source. For the carbon support, XC-72R is used. First, a solution of ethelyne glycol and water (75/25% by volume) was prepared in a 150mL beaker. The desired mass of precursor(s) was weighed in a sample tray. For sample calculations of required precursor see Appendix B. The tray was dipped into the glycol/water until all the precursor was dissolved or removed from the tray. Carbon (XC-72R) was then added to the solution. A stir bar was added to the beaker and the solution was vigorously agitated for 30 minutes. The stir bar was then removed and the slurry was transferred to a 500mL round bottom flask and then refluxed for 3 hours in open atmosphere. The catalyst was then collected on filter paper. Once the filtration was complete, the paper was dried in a vacuum for 8 hours at 70°C in nitrogen. The catalyst was collected by physically scraping it from the surface of the filter paper into a glass sample jar.

4.4 MEA Preparation Materials and Equipment

Membrane Electrode Assemblies(MEAs) studied in this work are all prepared in-house. They're composed of two catalyst coated GDLs, one for each electrode, and a Nafion membrane sandwiched in between them. The procedures for membrane pretreatment, catalyst application, MEA assembly and fuel cell operation are provided in this section. The MEA is made through hot pressing the electrodes and Nafion using a heated press. As is discussed in the electrode preparation procedure, the application of catalyst ink to anode and cathode GDLs required a vacuum oven for drying, and a mixing plate for catalyst ink-agitation.

4.4.1 Membrane Pretreatment

Membrane pretreatment is required to ensure proper proton conductivity. The proton exchange membranes used in this study are Nafion 112 for use with hydrogen, and Nafion 115 for use with alcohol. First, squares of untread Nafion(up to 5 per batch) membrane with dimensions 3" x 4" were made. Those squares were then placed in a 500mL beaker with 450mL of 3% hydrogen peroxide which was then brought to a boil using a hot plate. After 30 minutes a second 500mL beaker filled with 450mL of DI water was brought to a boil on a second hot plate. The Nafion was kept submerged in the boiling peroxide solution for 1 hour and then transferred to the boiling DI water. A solution of 1M sulfuric acid was then prepared in a 500mL beaker by adding 24mL of 99% sulfuric acid in 476mL of DI water and then brought to a boil. After an hour of being submerged in boiling DI water, the Nafion pieces were transferred to the boiling sulfuric acid solution. Finally, another 500mL beaker of 450mL DI water was brought to a slow boil and after an hour of boiling in 1M sulfuric acid, the membranes were transferred to the boiling DI water beaker and submerged for 1 hour. The membranes were then collected into an air tight jar filled with DI water for storage.

4.4.2 Electrode Preparation

When coated with catalyst, the GDL functions as an electrode in the fuel cell. To prepare catalyst ink, catalyst powder was measured using a high precision scale. The amount used was dependent on the loading of Pt desired.

For sample calculations please see Appendix B. For 0.4mg/cm^2 Pt loadings, 10mg of 20% Pt supported on carbon was required for each electrode. The catalyst was stirred to reduce agglomerates and it's mass was recorded. The catalyst was then added to a sample jar. To the jar 250mL of DI water, 250mg of n-propanol and 150mg of 10% Nafion ionomer solution were added and mixed with a metal spatula. For larger batches of catalyst, the liquid volumes were simply scaled up when making catalyst ink. A small magnetic stirrer was added to the jar, and placed in an ice bath over a stirring plate. The catalyst mixture was then stirred for an hour. Dry GDLs were cut with dimensions of 2.5" x 2.5". A vacuum oven was set to 80°C with a vacuum pump for a vacuum pressure of 15in-Hg. With a brush, the catalyst ink was lightly and uniformly coated on the GDLs and the GDLs were then placed in the vacuum oven for 15 minutes. Once the first coat was dried, the second coat was made perpendicular to the first, and the drying duration in the vacuum oven was reduced to 10min. With the second coat dried, two coats were applied to each GDL in a crosshatched pattern and then dried for 10min in the vacuum oven. This was repeated until no ink remained. The coated GDLs were weighed so that the catalyst loading achieved could be determined. The final step for electrode preparation was to coat the catalyst layer with Nafion solution. A solution of 75mg of 10% Nafion and 100mg of DI water was prepared in a small jar. One coat of the solution was applied to each electrode. The GDLs were dried in the oven and their final weight was recorded to determine the total catalyst and Nafon loading.

4.4.3 MEA Preparation

The MEAs in this study were prepared by hand using a heated press. First the anode GDL was laid on Teflon paper with the catalyst layer facing up. Treated Nafion was then positioned such that the electrode was in the center of the membrane. The cathode electrode was then placed, catalyst down, on the membrane, lined up with the anode GDL. Another Teflon gasket was placed on top, and the 'sandwich' of materials was placed between two metal plates in the heated press. The press was set to 150°C, and the MEA was pressed at 1000 pounds for 90 seconds. The plates were removed, and allowed to cool to room temperature before the MEA was recovered. The anode and cathode side were labeled, and if not immediately used, stored in a zip-lock bag.

4.4.4 Fuel Cell Operation

Once prepared, the MEA must go through a humidification conditioning to enhance membrane conductivity prior to conducting a performance test. Once installed in the fuel cell, the system is first purged with nitrogen. After purging, air and hydrogen feeds are turned on through the LabVIEW user interface. The MEA is first hydrated at low gas flow rates sufficient enough to draw 0.1 A/cm^2. Using higher flow rates will dry out the membrane and prevent it from hydrating. Cell temperature is also kept low at 25°C, while humidifier temperatures are maintained at 35°C. During this conditioning, the voltage is increased in steps, from 0 to 0.3V in 0.1V steps, with 30min between each step. After 2 hours, the Cell and Humidifier temperatures are increased slowly to the desired operating

temperatures. Once the temperatures are reached, the flow rates are adjusted to those required to produce 1A/cm^2. The system is allowed to operate at these conditions for 2 hours to ensure complete hydration of the membrane. Over that time, the cell voltage should improve and eventually stabilize. Once a steady state is reached, performance tests are performed. Air and hydrogen flow rates are maintained at 2 and 3 times stoichiometric requirements, respectively.

Chapter 5 : Results and Discussion

The objective of this study has been to understand PEM fuel cell operation and assess the viability of ethyl alcohol as a fuel through the evaluation of several electrocatalysts. In addition, an experimental system is used to study experimental parameters to maximize catalyst performance. The work in this thesis is specific to developing a basic understanding of catalyst activity and fuel cell optimization for the operation of a PEM fuel cell with a direct alcohol feed. The performances of the in-house developed catalysts are compared to published data in literature.

The experimental results of the study are presented in this chapter in three sections. The first section, 5.1, validates the operation of the fuel cell system with hydrogen or methanol as fuels. The second section, 5.2, discusses the process of evaluating and developing a catalyst synthesis procedure, and the performance validation of MEAs prepared using synthesized catalysts. The third section, 5.3, investigates potential sources of contamination detrimental to fuel cell performance.

Catalyst performance is evaluated through polarization, or V-I curves. The power output versus current density is also plotted and referred to as a power curve. In all fuel cell experiments, the gas and liquid flow rates were maintained as follows:

- H_2 is supplied at twice the stoichiometric requirement.
- Air is supplied at three times the stoichiometric requirement.

- Ethanol is fed at constant rates between 0.32 - 2mL/min.
- Methanol is fed at 2mL/min.

Initially characterization of the catalysts through X-ray Photoelectron Spectroscopy (XPS) was considered. Due to the nature of XPS being a surface chemistry measurement, and only penetrating the surface by 2 angstroms, the results were deemed inaccurate and omitted from the results. Additionally, preliminary half-cell tests were performed, but due to the limited number of samples tested the results were considered statistically insufficient. Instead, the mass composition of the catalysts was determined through a mass-balance of the raw precursor materials and collected catalyst.

5.1 PEM Fuel Cell System Reliability and Qualification

Before new catalysts can be synthesized and their reliability tested in the fuel cell, the repeatability of data in the experimental setup must be checked. This involved preparing two MEAs with a commercially available catalyst, and testing their performance in a hydrogen PEM fuel cell. Preparing MEAs and operating the fuel cell successfully and repeatedly is necessary prior to the testing of synthesized catalysts in the fuel cell system, as it rules out the operator or system as a source of error.

Following the MEA preparation procedure, MEAs for methanol and hydrogen operation are prepared. For hydrogen fuel, a target catalyst loading of 0.4mg/cm^2 is chosen, as is established in previous work to be an optimal loading[49]. Actual catalyst loading is 0.38mg/cm^2 in the finished MEA. Toray is chosen as the GDL, a paper based diffusion layer that is considered the industry standard. Nafion 112 pretreated by the procedure discussed in the previous sections is used as the membrane. Conditioning of the cell is conducted as per established procedure discussed earlier. The fuel cell is operated at 65°C, and humidification kept constant by maintaining a humidifier temperature of 75°C for both anode and cathode gases. The cell is operated at atmospheric pressure. The results of the validation test are shown in Figure 5.1. The curve A, in dark blue, represents the average results of two MEAs prepared in this study, and their respective variation (~5% maximum) represented by the vertical error bars. The curves labeled B and C are from two previous UNH studies using the same materials, fabrication and operating procedures[2,49].

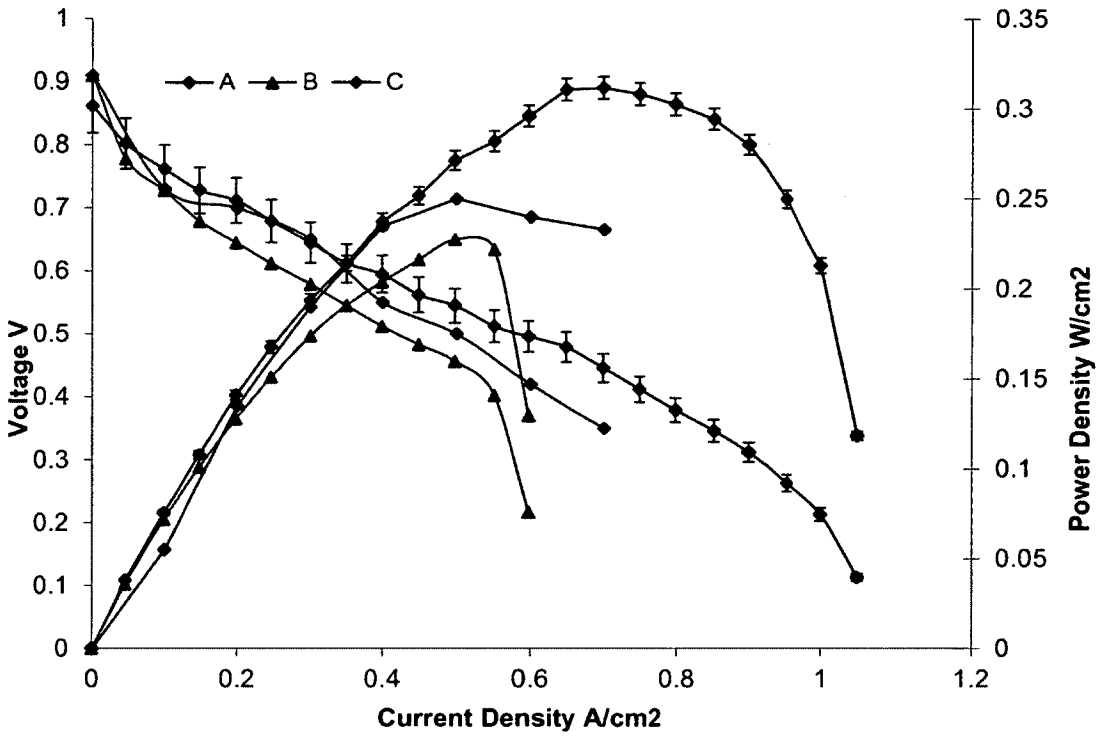

Figure 5.1: Hydrogren Operation Validation.
A=0.38mg/cm2 Pt, B= 0.32mg/cm2 Pt, C= 0.4mg/cm2 Pt. T=60°C, H2 Humidifier T=75°C, No Backpressure, Toray GDLs for Anode and Cathode.

The results shown in Figure 5.1 are very positive. The target Pt loading for all three MEAs was 0.4mg/cm^2. The differences in loadings may be related to the individual techniques used to paint the catalyst on the GDL. While the MEA preparation procedure is identical for A, B and C in Figure 5.1, the application of the catalyst layer to the GDL is unique for each MEA. The MEA in curve A had a catalyst loading 19% greater than B and 5% less than C. The MEA in curve A has a peak power density of ~0.3W/cm^2, 20% and 30% greater than the peak power densities for curves B and C, respectively. MEA A's improvement over MEA B is likely due to the increased loading.

The MEA in curve A achieved a peak power density of approximately 0.3W/cm^2 compared to the 0.25W/cm^2 maximum for the C MEA. The results also show the A MEA generated current density in excess of 1A/cm^2, while the B and C curves end prior to 0.8A/cm^2. The A curve implies that the MEA has lower ohmic and mass transport related overpotentials than the B and C MEAs. The activation overpotential seems slightly higher, as the open circuit voltage was 4% lower for the A curve. The test is repeated, and the results are within 1-2% for the two for the curve A.

A previous study using the same fuel cell system as that in this thesis work focused on optimization of experimental parameters for a direct methanol fuel cell(DMFC)[2]. Membrane electrode assemblies(MEAs) for methanol as fuel are different from those for hydrogen based fuel cells. In general, Pt-Ru is the standard catalyst for DMFC use, as it offers the best activity toward methanol electrooxidation. The DMFC study carried out in this lab previously is funded by Ballard Material Products for developing a GDL for use in DMFCs. The final product is a GDL material with a proprietary mirco porous layer. The newly developed GDL is used in the qualification testing in this study. The membrane used is Nafion 115. A catalyst loading of 2mg/cm^2 Pt-Ru is achieved using unsupported Pt-Ru black(50:50) catalyst. The cell is operated at 70°C using 4M MeOH solution at a feed rate of 2mL/min and a cathode back-pressure of 2atm. These conditions apply to all curves in Figure 5.2. The curve C represents performance data from a DMFC study from a collaborative research lab in China. Some of their methods and procedures are adapted to the DMFC study in this

laboratory[2]. Curve A is based on the average performance of two MEAs prepared in this study. Performance varied by a maximum of 2% between the two MEAs prepared and is represented by error bars.

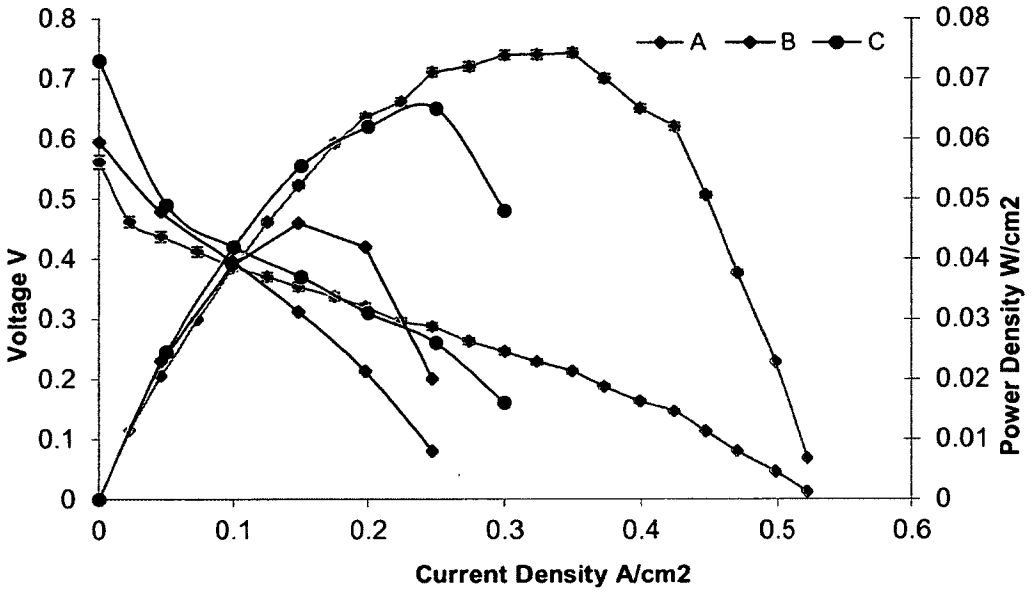

Figure 5.2: MeOH Operation Validation
A=1.63mg/cm2 PtRu, B=2mg/cm2 PtRu, C=2mg/cm2 PtRu, D=2mg/cm2 PtRu, E= ~2mg/cm2 PtR). T=70°C, 4M MeOH at 2mL/min, 2atm Cathode Backpressure, Ballard Material Products Anode and Cathode GDLs.

Curve A in Figure 5.2 achieved a peak power density of approximately 0.073W/cm^2, a 38% advantage over the results of the previous study, B(while the B curve has less than 2mg/cm^2 of catalyst, the target loading was 2mg/cm^2). This is easily explained through the use of optimized materials. The performance represented for the curve B is from in-house prepared MEA testing during the UNH DMFC study[2]. Since the intention is to verify proper MEA preparation and

cell operation, it only makes sense to relate the results to performance data of in-house prepared MEAs. Compared to the B and C MEAs, MEA A outperforms in all but open circuit voltage which is 150mV less compared to MEA C. The A MEA in Figure 5.2 exhibits greater activation overpotential versus the B and C MEAs. Ohmic and mass transport overpotentials appear the same for A, through the current density range 0.1-0.25A/cm^2. The performance for the A MEA, the power output is seen up to current densities of over 0.4A/cm^2. For the two MEAs prepared in this study that represent curve A, their performance is greater than those from previous work on the same test station [2]. The results for subsequent performance curves are based on average performance. Error bars are omitted due to the low standard deviation of the results.

5.2 Catalyst Synthesis and Evaluation

As this study is focused on the practical application of alcohol fuel cells, an effective method for catalyst synthesis is required. To accomplish this, a co-reduction synthesis procedure is chosen. The procedure by Spinace et al. [6] is a simple reduction of precursors in an ethylene glycol solution. To evaluate the synthesis, a well known Pt/C catalyst is first prepared.

Collection of prepared catalysts is conducted with a micron filtration paper. The filtration is tested for a carbon-water slurry and it is found that approximately 5% of the carbon is lost in the recovery process. Table 5.1 tabulates some of the previous work regarding catalysts for ethanol electrooxidation and DAFCs that influenced this study.

Table 5.1: Summary of catalysts from literature for DAFC use

Catalyst	Result	Source
Pt-Rh/C	Increased activity towards CO2 formation vs Pt/C, but lower reaction rates	[4]
Pt-Sn/C	Found the crystallinity of PtSn decreased with reduction in atomic ratio of Pt:Sn	[20]
Pt3Sn/C	Compared preparation methods. Presence of phosphorous increased catalyst performance.	[21]
PtRuSn/C	Sn-rich catalysts with SnO2 groups favored the overall oxidation of ethanol, and were more active towards C-C breakage	[5]
Pt-Ru/C, Pt-Rh/C	Pt monolayers were deposited on Ru/C and Rh/C. Results showed faster kinetics with Ru catalysts than with conventional catalysts(Pt/C).	[50]
Pt-Ru/C	Catalysts were prepared by co-reduction and showed alloying and small particle size addition to increase EtOH oxidation.	[6]
Pt3Sn2/C, Pt2Sn/C	Pt3Sn2/C performed best, at or above 90C, Pt2Sn/C performed significantly better.	[15],[19]
Pt-CeO2/C	Prepared catalyst offered better performance vs Pt/C for ethanol electrooxidation.	[51]
Pt-M/CuNi (M=Ru, Mo)	Pt-Mo/CuNi showed the highest performance, but charge transfer resistance across the surface of the catalyst was greater.	[25]
Pt-Ru/C	Voltammetry tests showed alloyed catalysts to be more active than pure platinum, with Pt52-Ru48/C giving the best performance.	[23]
PtRu/C, Pt3Sn/C	CO oxidation limitations were not an issue, but C-C breakage was.	[17]
Pt-RuO2-IrO2/C	Onset potential was reduced compared to PtRu/C catalysts.	[52]
PtSn/C, PtSnRu/C	Additon of Sn increased activity by several orders of magnitude. Acetic Acid was a reaction product for all catalysts.	[7]
Pt-RuO2/C	Produced higher current densities for ethanol electrooxidation than commercial Pt/C catalyst.	[8]
PtRuNi/C	Showed an activity towards ethanol electrooxidation ~5 times greater than PtRu/C.	[53]
Pd/MWCNT, C, carbon fiber	Multi-Walled carbon nanotube (MWCNT) supported Pd performed best.	[54]

Pd/TiO2	TiO2 supported Pd provided better performance over Pd/C.	[55]
Pt-Ru/Ni	For low current density application, low atomic% Ru was favored, and higher Ru for greater current densities.	[22]
Pt-CeO2/C, Pt-NiO/C, Pd-CeO2/C, Pd-NiO/C	Pd/C had a much higher activity towards ethanol oxidation in alkaline media compared to Pt. The binary oxides improved activity.	[9]
PtRu/C, PtSn/C, PtSnRu/C	PtSn/C provided the highest activity of all catalysts for methanol and ethanol oxidation. SnO2 was present in all Sn containing catalysts.	[10]
PtSn/C	Found that reaction products were primarily acetaldehyde and acetic acid.	[18]
PtM/C(M=Sn, Ru, Pd, W)	Pt Lattice parameters decreased with Ru/Pd and increased with Sn/W. In a single cell, PtSn/C showed the highest activities.	[24]
PtRuSn/C	Best catalyst had the ratio 60:10:30, and contained PtSn alloy and SnO2 structures, was capable of C-C breakage and acetic acid electrooxidation.	[11]
Pt3Te/C	Improved peak current density vs PtRu/C for ethanol electrooxidation.	[56]
Pd/Carbon Spheres	Activity improved 3 times compared to Pd/C.	[57]
PtPb/C, PtRuPb/C	At low potentials PtRuPb showed the highest activity, while no signs of metal alloying were evidenced.	[58]
Pd-NiO/C, Pt-NiO/C	Greater overpotential was discussed and noticed for CO oxidation on Pd, but the highest activity for ethanol electrooxidation was seen on Pd-NiO/C.	[12]
PtRh/C	Addition of Rh enhanced CO2 selectivity over Pt/C.	[26]

In the majority of the studies, the catalysts are evaluated in a half cell system. In addition, many of the catalysts require intricate or complicated synthesis procedures. The most promising catalysts in terms of performance, cost, and synthesis are platinum-tin based. Given that the purpose of the present study is to develop a basic understanding of DAFC fuel cells with respect

to catalysts, in addition to finding an effective catalyst, several Pt-Sn and Pt-Sn-Ru catalysts are prepared. In addition, synthesis of Pd based electrocatalysts is attempted, given the reported high activity of Pd toward ethanol electrooxidation versus platinum. The knowledge gained from preparation and evaluation of these catalysts can serve as a base for future studies of DAFCs at UNH and around the scientific world.

5.2.1 Pt/C Synthesis and Evaluation

Before complex binary or ternary catalysts are synthesized, the validation of the synthesis procedure is necessary. This is accomplished by MEA preparation and characterization using an in-house synthesized Pt/C catalyst. The performance is also compared to commercially available Pt/C, 20% Pt by weight, purchased from the Fuel Cell Store(www.fuelcellstore.com).

For all catalysts synthesized, a 20% Pt loading is chosen, both to allow direct comparisons with a commercial catalyst, and to minimize the Pt content of the catalyst. Situations where high Pt loadings in the MEA catalyst layer are desired pose a potential issue. These loadings are difficult to achieve through hand-painting due to the 80% carbon loading by weight, which results in a thick catalyst layer. The thickness of the catalyst layer required for Pt loadings over $1 mg/cm^2$ would sometimes cause cracking, flaking and poor adhesion to the GDL.

Initially a miscalculation caused of the higher than desired Pt loading. Once corrected, the Pt/C catalyst is synthesized again. It is assumed the

material retained in the filtration media is in the same ratio of the precursors added. It is determined that ~10% of the catalyst is retained in the filter paper based on tests with pure carbon in a glycol/water mixture. The mass of Pt/C collected is 24mg, based on a target Pt/C batch weight of 25g. This was repeated three times for Pt/C and approximately the same catalyst mass was recovered for each batch. Sample calculations for the catalyst mass balance can be found in Appendix B.

Three carbon support samples for catalyst synthesis are evaluated: 1) XC-72 carbon from China(Tsinghua University), 2) locally purchased XC-72 carbon heat treated in nitrogen at 600°C, and 3) XC-72 carbon heat treated in argon at 600°C. Three MEAs are then prepared with a Pt loading of 0.4mg/cm^2 and tested in a fuel cell. The results of the testing are presented in Figure 5.3.

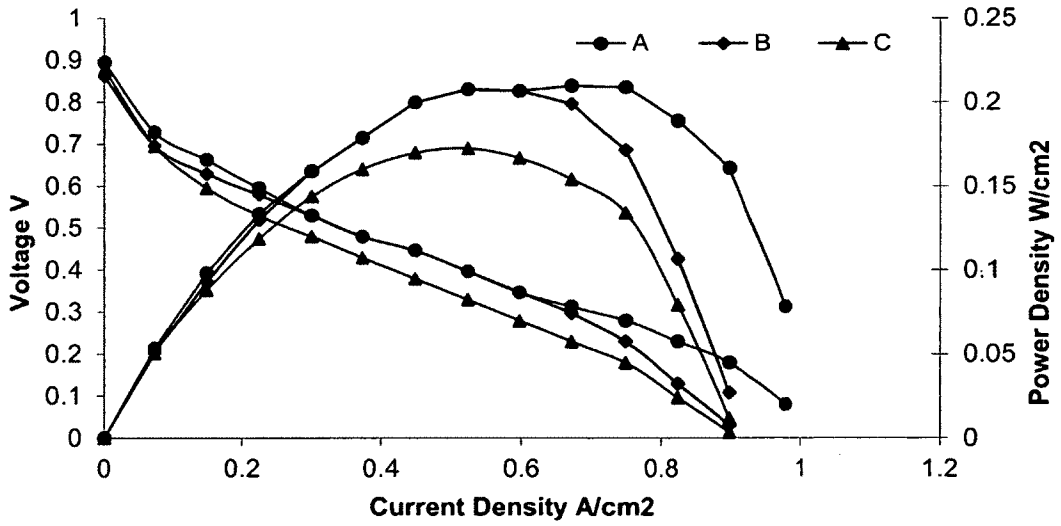

Figure 5.3: Carbon Support Evaluation
A=Carbon Supplied from lab in China, B=Carbon heat treated in N2, C=Carbon heat treated in Ar. Fuel Cell T=60°C, H2 Humidifier T=75°C, No Backpressure, 2x Stoich H2. Nafion N-112 Membrane,Toray GDL.

The performance shows that the catalysts using carbon heat treated in an N_2 atmposphere in our laboratory and carbon obtained from the laboratory in China achieved approximately the same peak performance. The catalyst supported on the China-supplied carbon shows superior performance at higher current densities. Given the results, the China-supplied XC-72R carbon is chosen as the support for all the subsequent catalysts synthesized in this study.

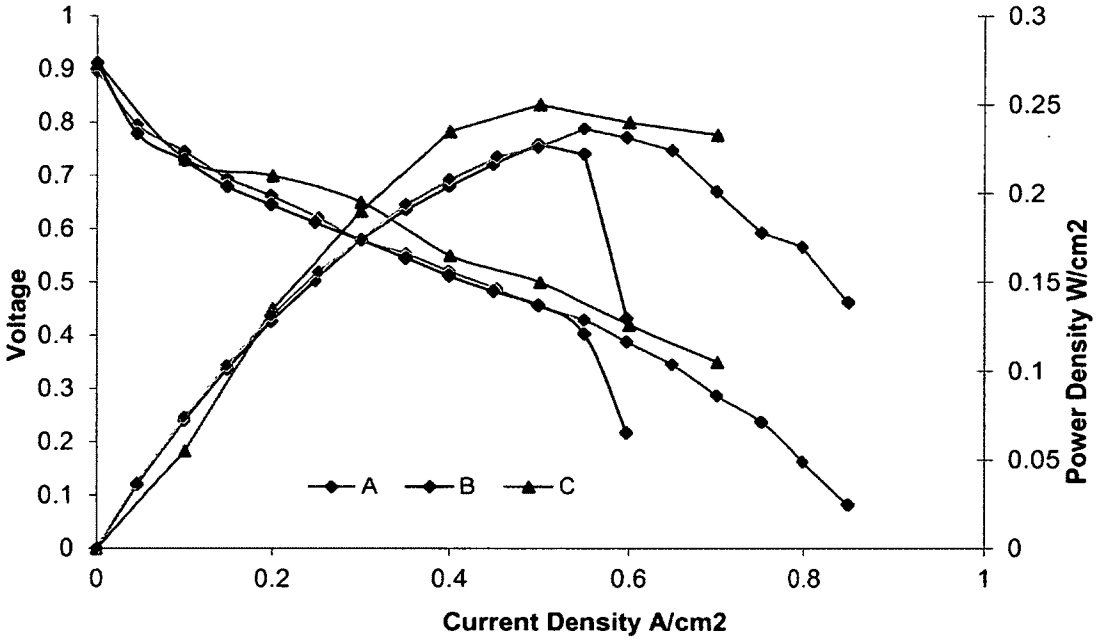

Figure 5.4: H2 Catalyst Evaluation
A=0.32 mg/cm2 Pt, 3.7atm backpressure, B=0.4mg/cm2 Pt, 1atm backpressure, C,D=0.4mg/cm2 Pt 1atm backpressure. T=60°C, H2 HumidifierT=75°C, 2x H2 Stoich. Membrane: Nafion 112, Toray GDL.

With the carbon support chosen, two batches of Pt/C are synthesized and tested twice using hydrogen as a fuel. The average results of two MEAs

prepared with in-house synthesized Pt/C catalyst are shown in Figure 5.4 as the A data points. Peak power densities of ~0.23W/cm^2 are observed. The peak power measured with the A MEA nearly matches the peak measured by a previous in-house study[49], represented by the curve C. It should be noted, curve C is measured using the first generation, manual fuel cell system at the University of New Hampshire. The synthesized catalyst also outperforms an MEA from a more recent in-house study represented by the curve B[2]. Both the B and C curves are obtained from MEAs using commercially available Pt/C(20% Pt by weight). The purpose for the comparisons is to illustrate the relative performance of the synthesized catalyst in this study versus a previous study using the same fuel cell system, components, materials and procedures. The results of the performance test show the in-house synthesized catalyst performance is essentially equivalent to the results obtained through previous studies using a commercial Pt/C catalyst. The average performance represented by curve A in Figure 5.4 validate our catalyst synthesis procedure.

With the catalyst synthesis procedure validated for hydrogen PEM fuel cell operation, the next step was to prepare catalysts for DAFC use. Table 5.2 lists the various catalysts to be synthesized and their respective target compositions by atomic ratios.

Table 5.2: List of Synthesized Catalysts and their Atomic Compositions

Catalyst		Atomic Composition				Weight %				
		Pt	Sn	Ru	Pd	Pt	Sn	Ru	Pd	C
A	Pt/C	1				20				80
B	PtSn/C	1	1			20	12			68
C	Pt_2Sn/C	1	0.5			20	6			74
D	$PtSnRu_{0.5}/C$	1	1	0.5		20	12	5		63
E	$PtSn_{0.5}Ru/C$	1	0.5	1		20	6	9		65
F	Pt2SnRu/C	1	0.5	0.5		20	6	5		69
G	PtSnRu/C	1	1	1		20	12	9		59
H	Pd/C				1				30	70
I	PtPd/C	1			1	20			18	62
J	$PtPd_{0.5}/C$	1			0.5	20			9	71
K	$PtSn_{0.5}Pd/C$	1	0.5		1	20	6		17	57
L	Pt_2SnPd/C	1	0.5		0.5	20	6		8.5	65.5

Each catalyst in Table 5.2 has a platinum loading of 20% by weight and is supported on XC-72R carbon from China. Due to time and synthesis issues, catalysts G and I through L are not prepared. Several batches of catalysts A through H are prepared in this study and evaluated through XPS and single cell PEM fuel cell tests. Each catalyst is evaluated using both hydrogen and ethyl alcohol as fuel. For ethyl alcohol, multiple flow rates and temperatures are studied in an attempt to determine optimal operating conditions for each catalyst.

As mentioned, the catalysts were chosen based on the results from the various studies in Table 5.1. Time constraints reduced the total number of catalysts tested. With the synthesis validated through Pt/C evaluation, the binary and ternary catalysts are prepared.

Preparation of MEAs from the synthesized catalyst is the next step. Table 5.3 lists the 6 catalysts successfully synthesized for this DAFC study.

Table 5.3: Synthesized carbon supported catalysts and their atomic ratios

	Atomic Ratio of Metal			
Catalyst	Pt	Sn	Ru	Pd
A(Pt/C)	1			
B(PtSn/C)	1	1		
C(Pt_2Sn/C)	1	0.5		
D($PtSnRu_{0.5}$/C)	1	1	0.5	
E($PtSn_{0.5}Ru$/C)	1	0.5	1	
F(Pt_2SnRu/C)	1	0.5	0.5	
H(Pd/C)				1

5.2.2 Synthesized Catalysts Performance With H_2

The MEAs prepared with the synthesized catalyst had a loading of 1mg/cm^2 Pt, or Pd, using a proprietary GDL developed at UNH for Ballard Material Products, and Nafion N-115 as the membrane. The default test conditions are 75°C cell temperature, 1ml/min flow of 1M EtOH, with air flow at a rate 3 times the stoichiometric requirement and a cathode backpressure of 2 atm. Experiments with additional temperatures and pressures are also conducted, but in most cases the performance of the DAFC is unsatisfactory.

Before the catalysts are tested with ethanol, their performance is first measured with hydrogen. The results of the hydrogen tests for the catalysts in Table 5.3 are given in the polarization(Fig. 5.5) and power curve(Fig 5.6). MEA specifications for Figures 5.5 and 5.6 are given in Table 5.4.

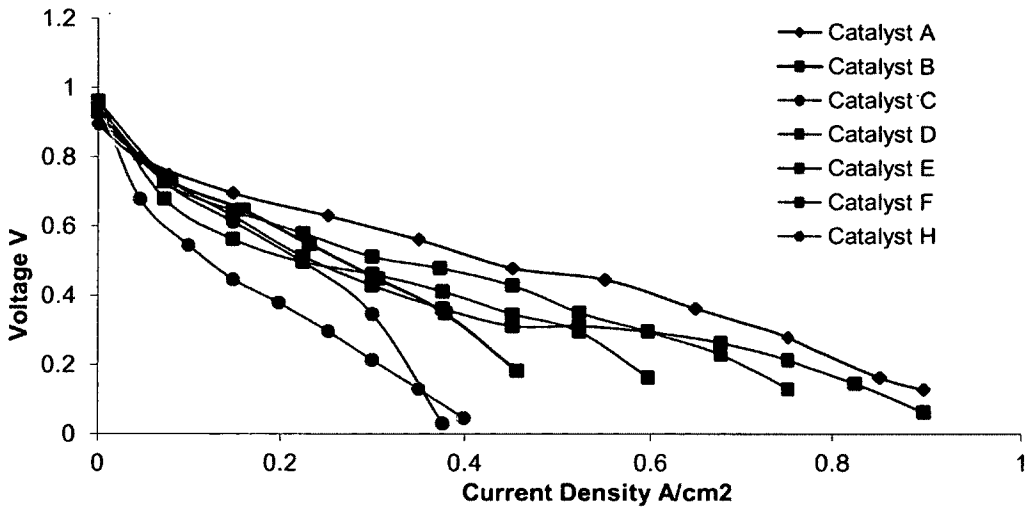

Figure 5.5: H2 V-I Curves for Synthesized Catalysts.
Fuel Cell T=65C, Anode/Cathode Humidification T=75C
2x Stoich H2, 3x Stoich Air.

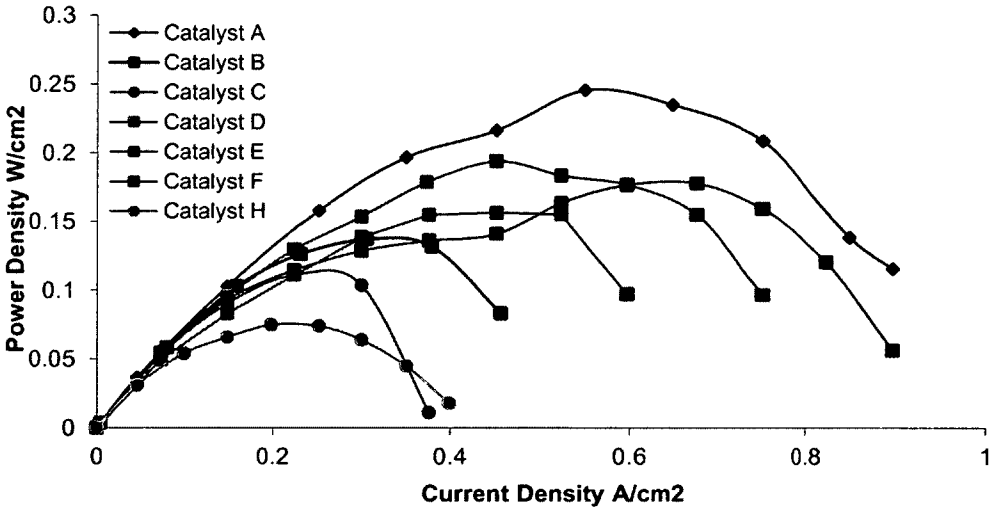

Figure 5.6: H2 Power Curves for Synthesized Catalysts..
Fuel Cell T=65C, Anode/Cathode Humidification T=75C
2x Stoich H2, 3x Stoich Air.

Table 5.4 : MEA configuration for Figures 5.5 & 5.6

Catalyst	Membrane	Anode Pt loading (mg/cm^2)	Cathode Pt loading (mg/cm^2)	Anode GDL	Cathode GDL
A	N-112	0.4	0.4	Toray	Toray
B-F	N-115	1	0.4	Ballard	Toray
H	N-115	1(Pd)	0.4	Toray	Toray

In theory, the synthesized ethanol catalysts should yield performance data in a hydrogen PEMFC at the same or lower level when compared to the synthesized Pt/C catalyst (Catalyst A) performance. While the platinum mass composition is the same for each catalyst at 20% by weight, the desired platinum loading for the MEAs in a DAFC is $1mg/cm^2$, more than double the $0.4mg/cm^2$ loading required in a hydrogen PEMFC . For all MEAs, the catalyst on the cathode is a commercial 20% Pt/C catalyst. The oxygen reduction reaction at the cathode does not necessitate complex binary or ternary electrocatalysts.

The 20% platinum mass composition of the DAFC catalysts (B-F) means that a thick catalyst layer is required for a platinum loading of $1mg/cm^2$. The increased thickness can impede diffusion to the membrane as well as block pores in the GDL and increase contact resistance. In practice, the DAFC catalysts (B-H) perform at nearly the same level, with the outliers being catalysts B, C and H. The reduced performance of the catalysts B and C (PtSn/C and Pt_2Sn/C) may be due to the reduced activity of tin toward hydrogen reduction compared to platinum or ruthenium. Catalysts D, E and F exhibit performance in

line with what was expected, performance seems to drop off due to mass transport limitations, as discussed in Chapter 2. A combination of catalyst loading differences, catalyst surface inconsistencies and the presence of ruthenium may be the source of the variances in performance. The palladium catalyst shows the lowest performance, which will be discussed later on.

5.2.3 Catalyst B

Catalyst B (PtSn 1:1) yielded some of the highest performance in this study at 75°C, shown in Figure 5.7. In a DAFC the catalyst allowed the cell to achieve a peak power density of just over 10mW/cm^2 at an operating temperature of 75°C. At the same temperature the cell produced power at 80mA/cm^2, matching the 80°C measurement of Catalyst E(Figure 5.12).

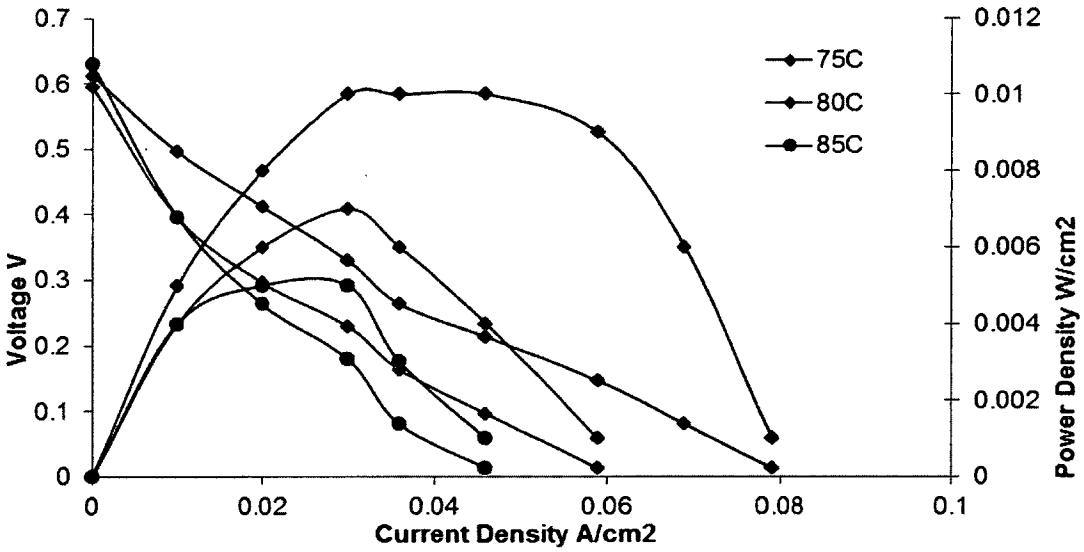

Figure 5.7: Catalyst B EtOH performance curves.
No humidification. Membrane: N-115.
Anode: 1mg/cm2 20% Pt, 1ml/min 1M EtOH sol., Ballard GDL
Cathode: 0.4mg/cm2 20% Pt/C, 3x Stoich Air, Toray GDL

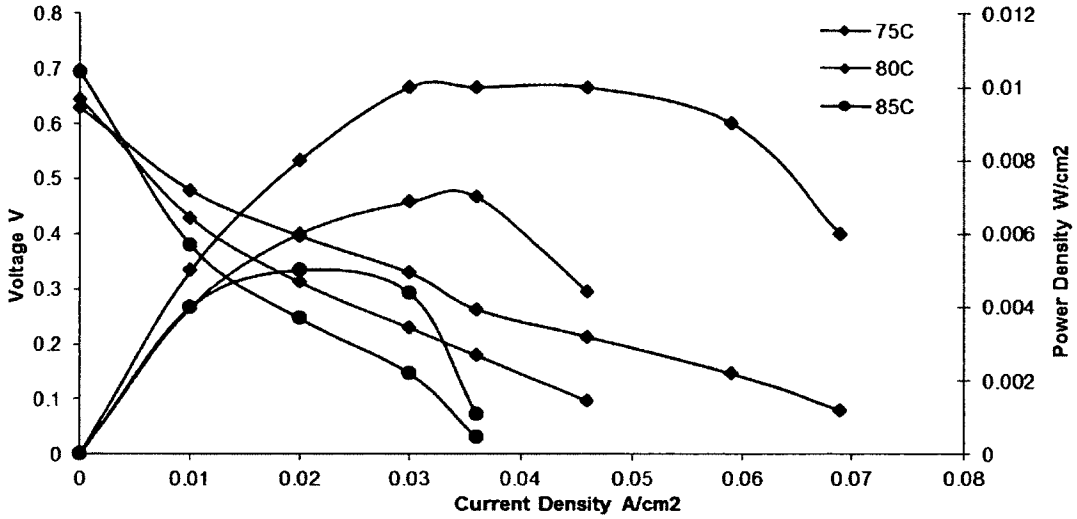

Figure 5.8: Catalyst B low flow rate EtOH performance curves.
No humidification. Membrane: N-115.
Anode: 1mg/cm2 20% Pt, 0.32ml/min 1M EtOH sol., Ballard GDL
Cathode: 0.4mg/cm2 20% Pt/C, 3x Stoich Air, Toray GDL

Low fuel flowrate(0.32ml/min) testing for Catalyst B achieved the same 10mW/cm^2 peak power density at 75°C shown in Figure 5.8. This is similar to the results at 1ml/min at the same temperature (Fig. 5.7). At 75°C, the cell failed to sustain power beyond 60mA/cm^2, a decrease by 10mA/cm^2 against the results at a flow rate of 1ml/min. This is due to diffusion limitations, which is seen by the sharp decrease in power at 60mA/cm^2.

5.2.4 Catalyst C

Catalyst C (Pt_2Sn/C) provides the highest peak power density, 11mW/cm^2 of all of the DAFC catalysts tested(Fig. 5.9). This peak is achieved at both 75°C and 85°C. The peak power density is reached sooner at 75°C, though power

output could not be sustained beyond 80mA/cm^2. Results at 85°C show power output extending to 90mA/cm^2, the highest for the DAFC catalysts tested in this study. The poor results at 80°C may be due to experimental error, as the performance is much lower compared to the other set of results for temperatures of 75 and 85°C.

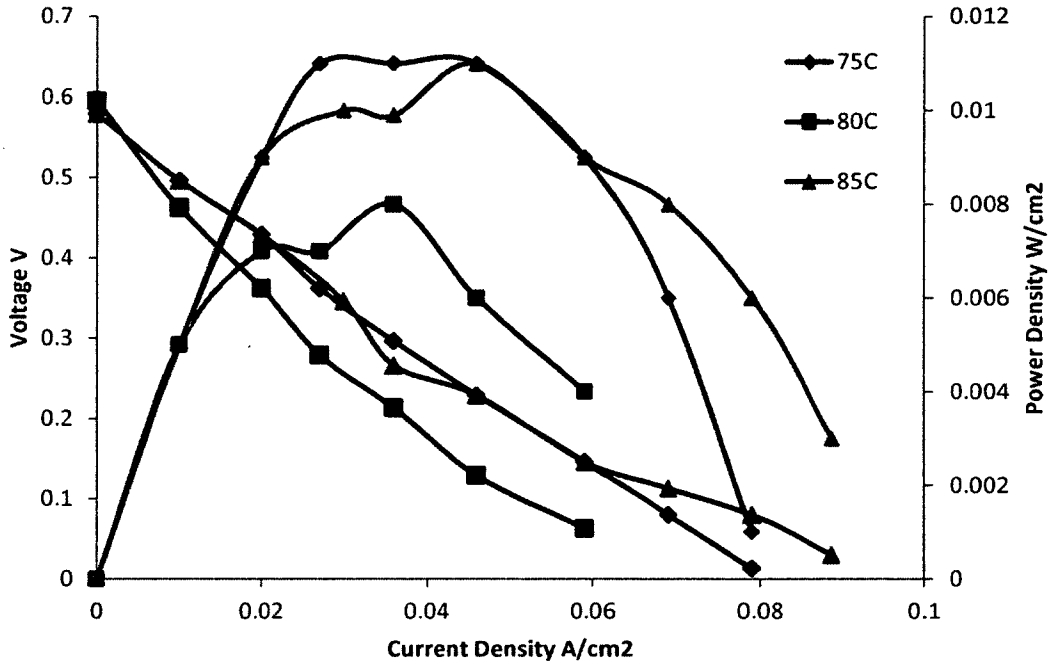

Figure 5.9: Catalyst C EtOH performance curves.
No humidification. Membrane: N-115.
Anode: 1mg/cm2 20% Pt, 1ml/min 1M EtOH sol., Ballard GDL
Cathode: 0.4mg/cm2 20% Pt/C, 3x Stoich Air, Toray GDL

At a lower fuel flowrate of 0.32ml/min(Fig. 5.10), Catalyst C maintains the same peak power density of 11mW/cm^2 that is measured with an ethanol flowrate of 1ml/min. However, the reduced flow impedes the ability of the fuel cell to output power beyond 80mA/cm^2, a reduction of 10mA/cm^2 as compared to

a flow rate of 1ml/min. Figure 5.10 shows approximately the same response to temperature as for 1ml/min in Figure 5.9. The performance increased with increasing temperature. In the case of low flowrate, the cell performance is clearly greater at 85°C. This is likely due to reduced mass transport resistance of intermediate species and effluent gasses leaving the system because at this temperature the feed is almost completely vaporized in the fuel cell.

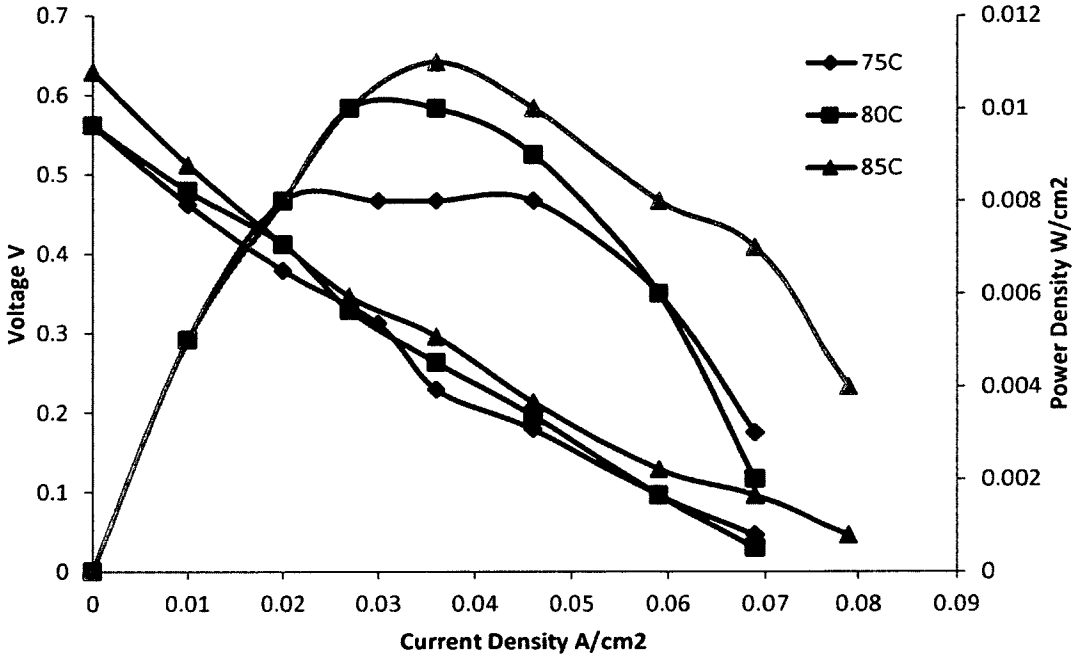

Figure 5.10: Catalyst C low flow rate EtOH performance curves.
No humidification. Membrane: N-115.
Anode: 1mg/cm2 20% Pt, 0.32ml/min 1M EtOH sol., Ballard GDL
Cathode: 0.4mg/cm2 20% Pt/C, 3x Stoich Air, Toray GDL

5.2.5 Catalyst D

Catalyst D (PtSnRu/C 1:1:0.5) performs similar to Catalys F in the hydrogen PEMFC but shows higher performance in a DAFC. At 75°C the maximum power density measured is ~33% greater than Catalyst F with 8mW/cm^2. Figure 5.11 and 5.15 shows that Catalyst D is similar to Catalyst F in that an increase in temperature cause a decrease in performance. The slight drop in peak performance between 0.020 - 0.030A/cm^2 suggest that at that temperature condition, the cell might need more time to reach a steady state.

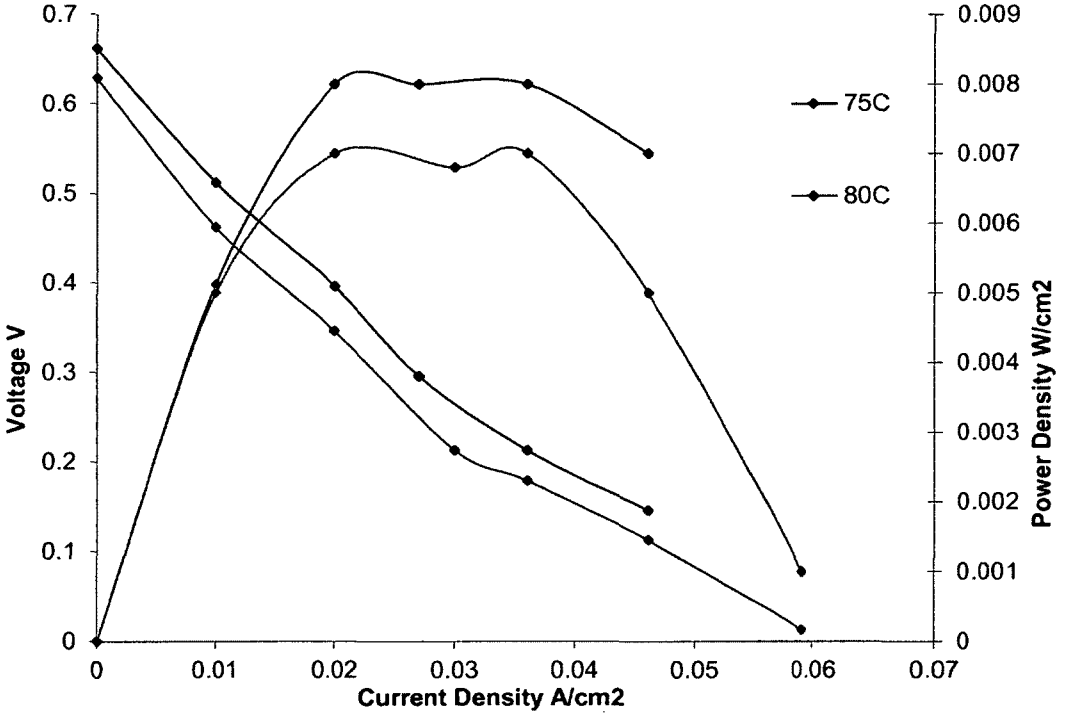

Figure 5.11: Catalyst D EtOH performance curves.
No humidification. Membrane: N-115.
Anode: 1mg/cm2 20% Pt, 1ml/min 1M EtOH sol., Ballard GDL
Cathode: 0.4mg/cm2 20% Pt/C, 3x Stoich Air, Toray GDL

The addition of ternary Ru at an atomic ratio of half that of platinum did not improve upon the DAFC performance compared to the binary platinum-tin catalyst B, and C.

5.2.6 Catalyst E

Catalyst E (PtSnRu/C 1:0.5:1) performs the lowest of the ternary catalysts in the hydrogen fueled test(Fig. 5.5). Under DAFC operation the catalyst performs the highest of the three ternary catalysts(Figures 5.12 - 5.14), achieving about 9mW/cm^2 as a peak power density and the catalyst maintained power output up to 70mA/cm^2, whereas Catalyst D had previously maintained power up to only 60mA/cm^2. Like Catalyst F (Figure 5.15), OCV is greater at higher temperature. Performance is very similar at 75 and 80°C, but was lowest at 85°C. The rapid drop in performance at 85°C may be a physical limitation of the thick catalyst layer being unable to quickly allow diffusion of fuel in the gas phase.

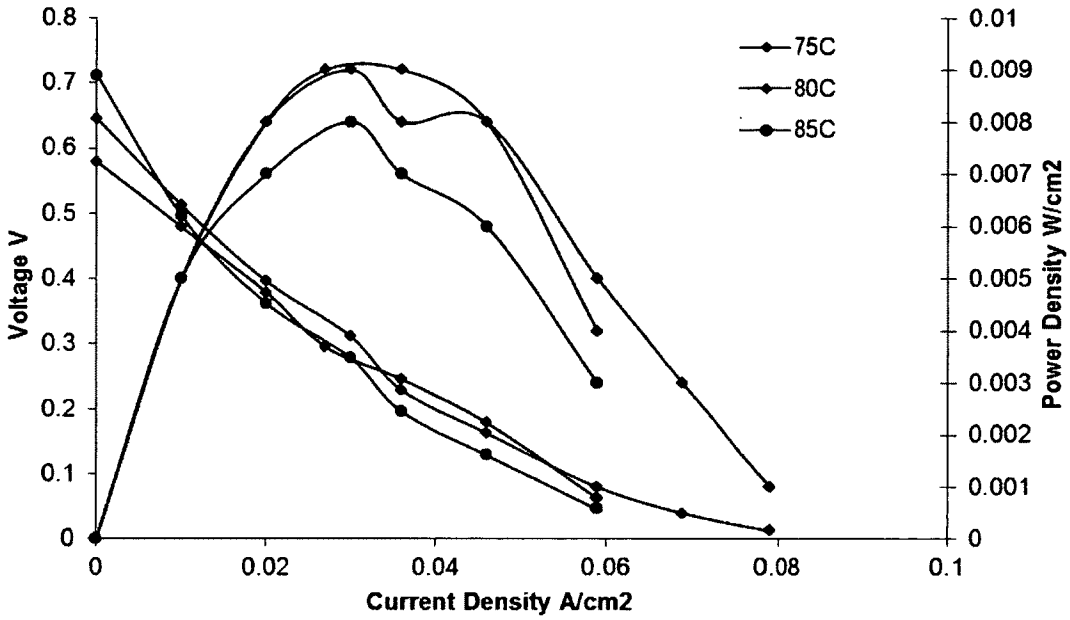

Figure 5.12: Catalyst E EtOH performance curves.
No humidification. Membrane: N-115.
Anode: 1mg/cm2 20% Pt, 1ml/min 1M EtOH sol., Ballard GDL
Cathode: 0.4mg/cm2 20% Pt/C, 3x Stoich Air, Toray GDL

In another set of experiments performance is measured at the lower fuel flow rate of 0.32ml/min of ethanol and then a higher flow rate of 2ml/min. The results in Figure 5.13 for lower flow rate, show a peak power density of 10mW/cm2, an improvement in peak power, but at the cost of reduced power output. At the lower flow rate, the cell could not provide measurable power output beyond 60mA/cm2. In this case the lower temperature shows poor performance. The ~15mV difference at OCV between the 75°C and 85°C condition is expected given the direct relationship between reaction kinetics and temperature.

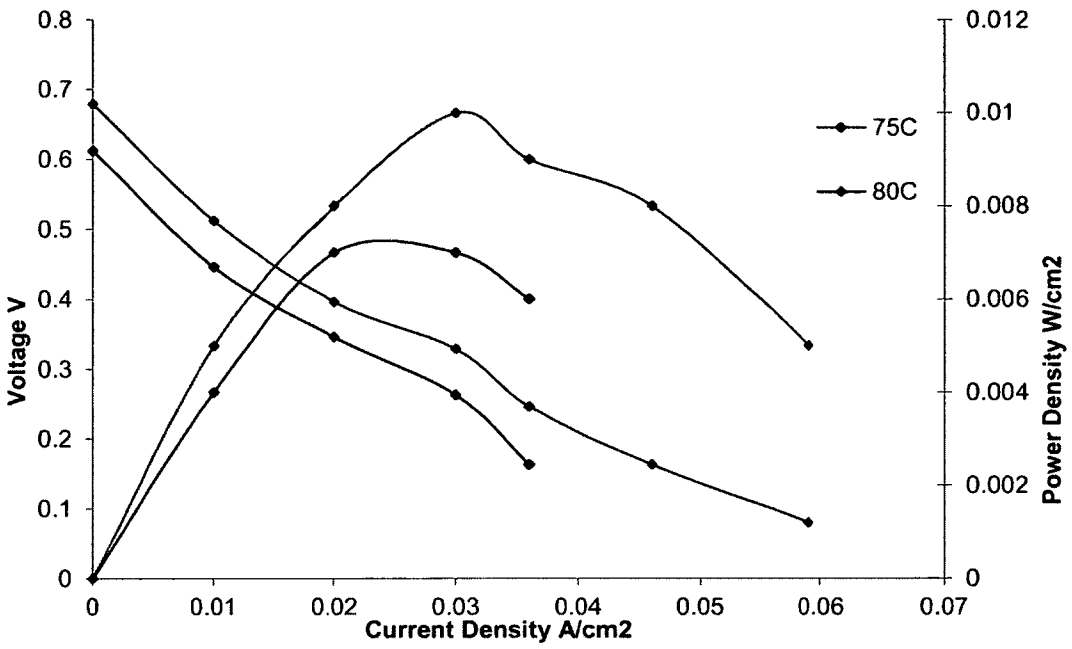

Figure 5.13: Catalyst E low flow rate EtOH performance curves.
No humidification. Membrane: N-115.
Anode: 1mg/cm2 20% Pt, 0.32ml/min 1M EtOH sol., Ballard GDL
Cathode: 0.4mg/cm2 20% Pt/C, 3x Stoich Air, Toray GDL

Cell performance measured at a flow rate of 2ml/min is presented in Fig. 5.14. It shows the same trend as for 0.32ml/min(Fig. 5.13). Overall performance increased with an increase in cell temperature. The peak performance at 2ml/min is observed to be 10mW/cm^2 at 85°C, 1mW/cm^2 greater than the performance observed at a flow rate of 1mL/min. At this high rate of flow both the anode and cathode would experience different conditions that inhibit performance. At the anode flooding might occur; additionally, the counter flow of the fuel and intermediates might impede diffusion to and from the catalyst surface. At the cathode, a higher air flow rate would be required, such rates

could cause a drying effect on the membrane; additionally, with an increased fuel flow rate, an even greater concentration gradient could exist to drive ethanol crossover through membrane.

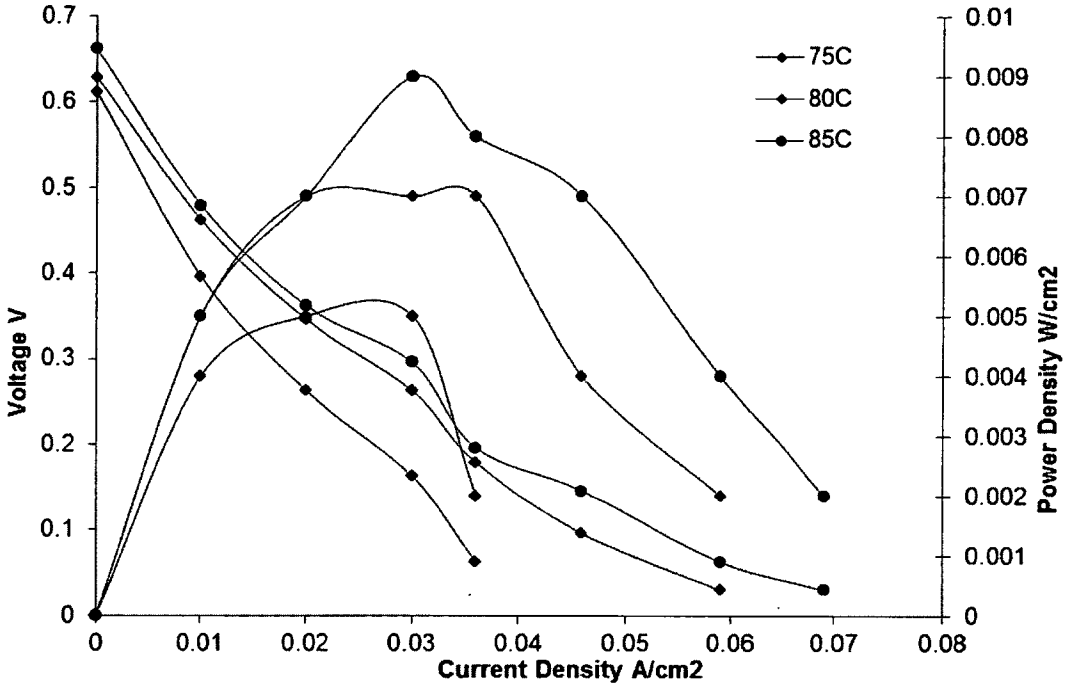

Figure 5.14: Catalyst E high flow rate EtOH performance curves.
No humidification. Membrane: N-115.
Anode: 1mg/cm2 20% Pt, 2ml/min 1M EtOH sol., Ballard GDL
Cathode: 0.4mg/cm2 20% Pt/C, 3x Stoich Air, Toray GDL

The reduction in tin content and increase in ruthenium allows Catalyst E to gain about 1mW/cm^2 of peak power. The catalyst still lags behind the peak performance of the two binary platinum-tin catalysts, B and C.

5.2.7 Catalyst F

The performance of Catalyst F (Pt_2SnRu/C 1:0.5:0.5) in a hydrogen fueled PEMFC as shown in Figures 5.5 and 5.6, makes it one of the top two catalysts in this study. Figure 5.15 shows the performance of the catalyst in a DAFC. The first notable trend is the performance decreasing with increasing temperature. Above 75°C the ethanol solution begins to vaporize. Given the decreasing performance at 80°C and 85°C this catalyst may not be effective for a mixed phase fuel. It is also possible that the catalyst layer is causing some overall overpotential loss, both ohmic and diffusion based, due to its thickness. The activation overpotential is decreasing with increasing temperature, an expected effect of high temperature on kinetics. In the case of Catalyst F, the addition of ternary ruthenium does not appear to improve the catalyst performance in a DAFC.

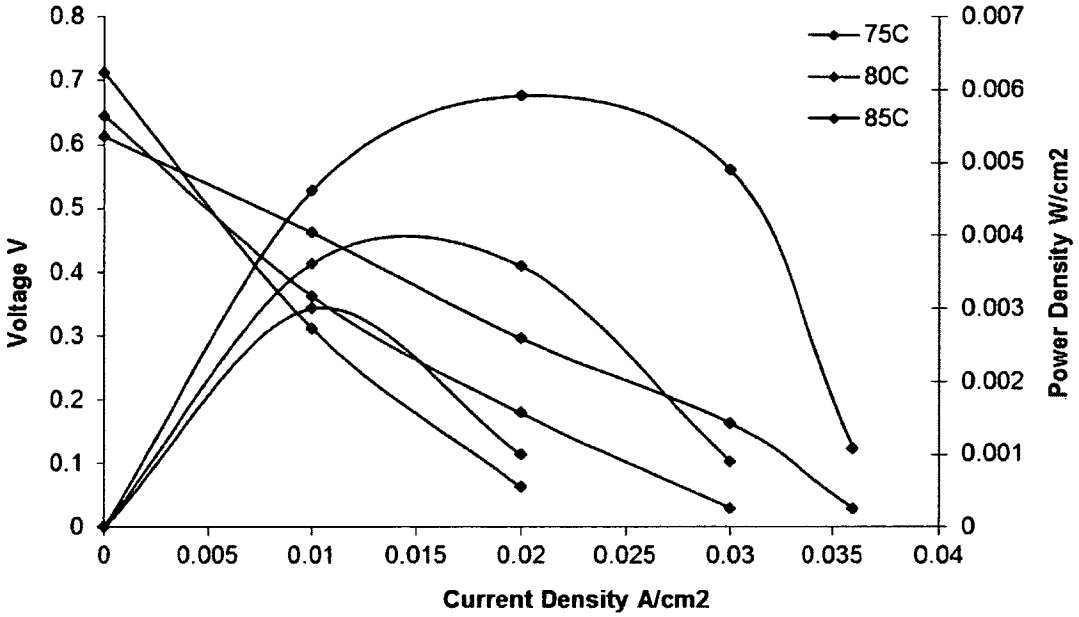

Figure 5.15: Catalyst F EtOH performance curves.
No humidification. Membrane: N-115
Anode: 1mg/cm2 20% Pt, 1ml/min 1M EtOH sol., Ballard GDL
Cathode: 0.4mg/cm2 20% Pt/C, 3x Stoich Air, Toray GDL

The reduction in ternary tin and ruthenium in Catalyst F, compared to Catalysts D and E appears to have reduced its overall performance in a DAFC significantly. While this study shows binary platinum-tin catalysts to have greater DAFC performance compared to ternary platinum-tin-ruthenium catalysts, an optimum ternary composition may exist that includes ruthenium in a higher concentration than was considered in this study.

5.2.8 Catalyst H

Catalyst H (Pd/C) is prepared and intended to be a precursor to additional catalysts, both binary and ternary featuring palladium. In spite of the time and efforts spent for synthesis, the catalysts never achieved the desired loading of 40% Pd supported on carbon. The alcohol reduction synthesis needed modification to reduce the palladium precursor, $PdCl_2$. The procedure is modified by introducing hydrochloric acid when a new synthesis is attempted. Several batches of Pd/C were prepared and performance was measured in the PEMFC. Unfortunately the power output was nearly immeasurable, so an alternative synthesis method was attempted.

The procedure is taken from literature[59]. First a solution of 8.25g palladium chloride in 5mL of hydrochloric acid in 50mL of DI water was prepared. The solution was cooled in an ice-salt bath where 50mL of 40% formaldehyde and 11g of acid-washed activated charcoal was added. The mixture was stirred mechanically while a solution of 50g potassium hydroxide in 50mL of water was added. The solution was kept below 5°C at this stage in the synthesis. Once the addition was completed, the temperature of the solution was raised to 60°C for 15 minutes. The catalyst was washed by decantation with water, and then again with dilute acetic acid. The catalyst was collected on a Buchner filter where it was washed with water several times. The catalyst was then dried at 100°C and stored in a desiccator.

Synthesis of Pd/C is attempted several times using this procedure. With this catalyst, synthesis of a Pd-Pt/C catalyst is attempted. Unfortunately, almost zero measurable cell performance is observed and a performance curve could not be made.

However, single cell PEMFC testing of the Pd/C catalyst prepared by the alternative synthesis method was conducted with hydrogen as a fuel. The result of the testing is given in Figure 5.16.

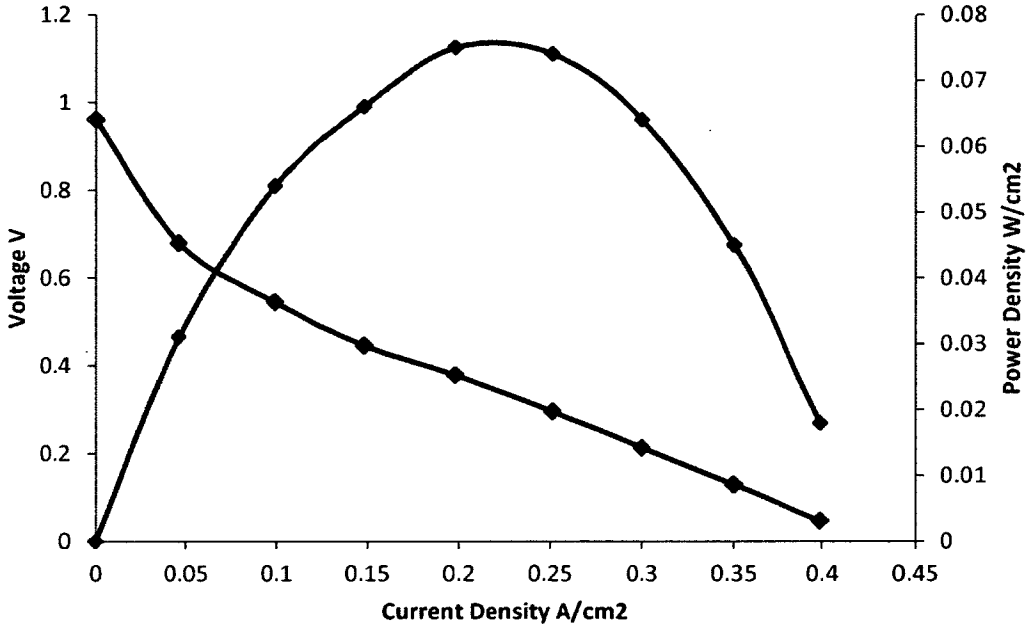

Figure 5.16: Catalyst F PEM performance with Hydrogen. GDL:Toray. Fuel Cell T=65C, 1mg/cm2 Pd, Cathode: 0.4mg/cm2 Pt/C, Anode/Cathode Humidification T=75C, 2x Stoich H2, 3x Stoich Air. N-112 Membrane.

The measured power density as shown in Figure 5.16 is approximately 77% lower than that of 20% platinum on carbon. Lower performance compared to platinum was expected using hydrogen as fuel.

It has been reported that Palladium has a much greater ability to oxidize ethanol in an alkaline media compared to platinum[9], but due to Nafion® sensitivity, the same 1M EtOH and water solution is used to test Pd/C in a DAFC. When operated as a DAFC, the Pd/C containing MEA produced no measurable power output. This is potentially a limitation of Pd, as it may not be suited to oxidize ethanol in a non-alkaline solution on its own. A binary or ternary catalyst containing Pd may be required. Additional causes for poor performance will be discussed later on in this chaper.

5.2.9 Temperature Study

Figures 5.17 and 5.18 provide a comparison of some of the catalysts for the different temperatures used in this study. At an operating temperature of 75°C, the highest performing catalyst is Catalyst C, achieving a peak power density of 11mW/cm^2, which is 1mW/cm^2 greater than the other binary platinum-tin catalyst, Catalyst B.

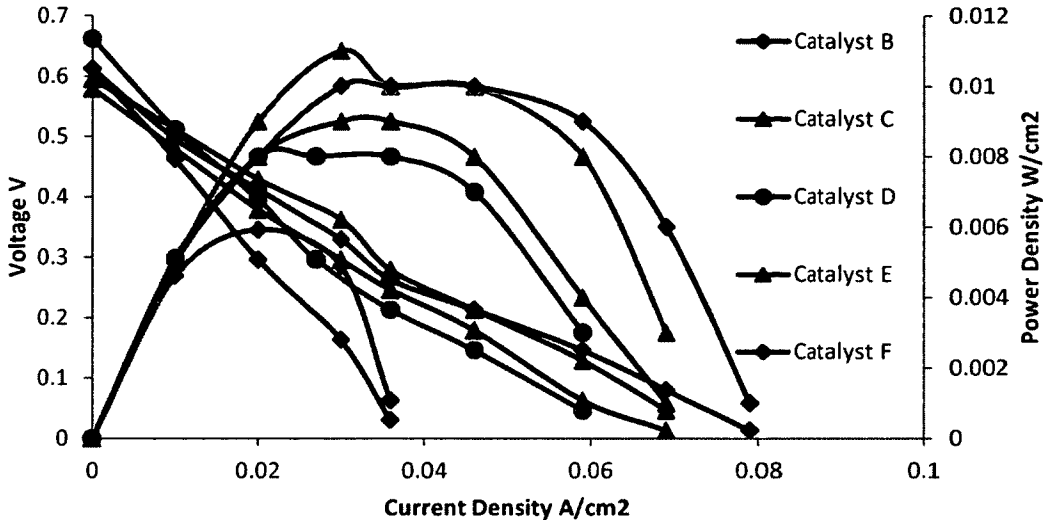

Figure 5.17: Catalyst B-F EtOH performance at 75°C.

No humidification. Membrane: N-115.

Anode: 1mg/cm2 Pt, 1ml/min 1M EtOH sol., Ballard GDL

Cathode: 0.4mg/cm2 20% Pt/C, 3x Stoich Air, Toray GDL.

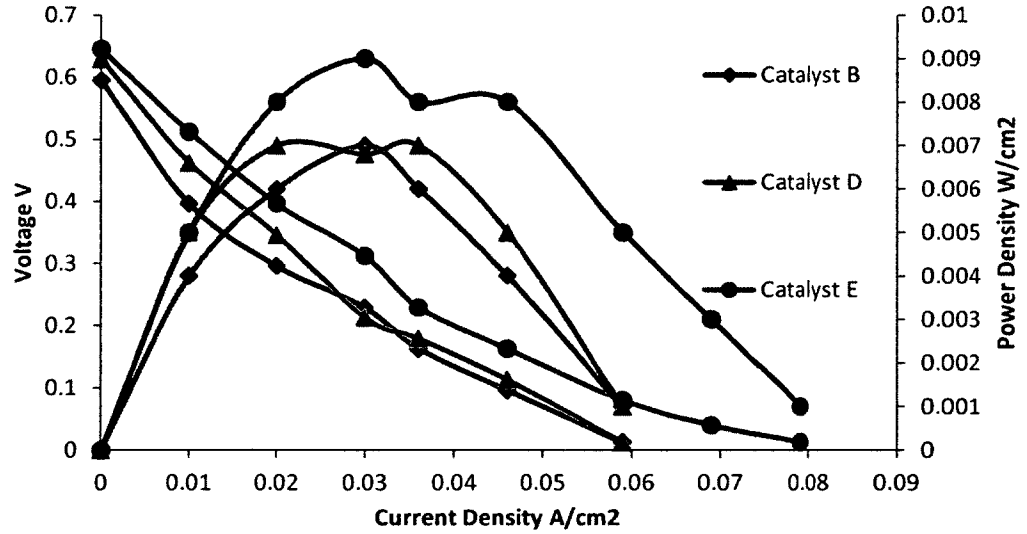

Figure 5.18: Catalysts B, D & E EtOH performance at 80°C.

No humidification. Membrane: N-115.

Anode: 1mg/cm2 Pt, 1ml/min 1M EtOH sol., Ballard GDL

Cathode: 0.4mg/cm2 20% Pt/C, 3x Stoich Air, Toray GDL

At 80°C the maximum performance is achieved with Catalyst C. At this temperature, the performance of most of the catalysts studied is unstable. As a result, curves are only present for catalysts B,D and E in Figure 5.18. Compared to results at 75°C, the peak power density is approximately 9mW/cm^2 for Catalyst B, 2mW/cm^2 lower than the peak power observed at 75°C of 11mW/cm^2 for Catalyst C. This could be due to the mixed liquid and gas phase of the fuel at 80°C. The maximum current density observed is 80mA/cm^2 for Catalyst C, while mass transport limitations reduce the maximum current density for Catalysts B and D to 60mA/cm^2.

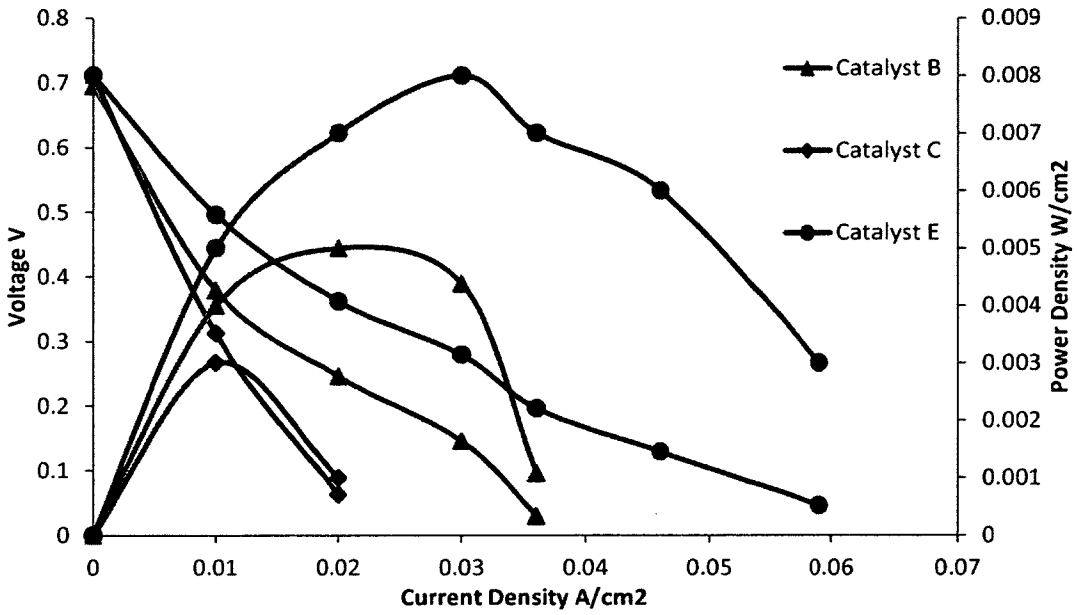

Figure 5.19: Catalysts B,C & E EtOH performance at 85°C.
No humidification. Membrane: N-115.
Anode: 1mg/cm2 Pt, 1ml/min 1M EtOH sol., Ballard GDL
Cathode: 0.4mg/cm2 20% Pt/C, 3x Stoich Air, Toray GDL

Due to the unstable performance at 85°C, the results at that temperature are limited to Catalysts B, C and E in Figure 5.19. In theory, the higher

temperature should increase peak performance, but in general this was not the case. It may be that the GDL and catalyst layers in this study respond better to a liquid feed rather than a feed that is mostly vapor, which is what would be present at 85°C operating temperature with 1M EtOH.

5.3 Low Performance Troubleshooting Tests

In all of the polarization curves, one characteristic is obvious, the peak power density is never greater than 10-11mW/cm2. Literature values have Pt-Sn electrocatalysts achieving power densities five times those recorded in this study, as high as 60mW/cm^2[21, 23]. Hydrogen PEM tests are revisited to investigate this apparent limitation.

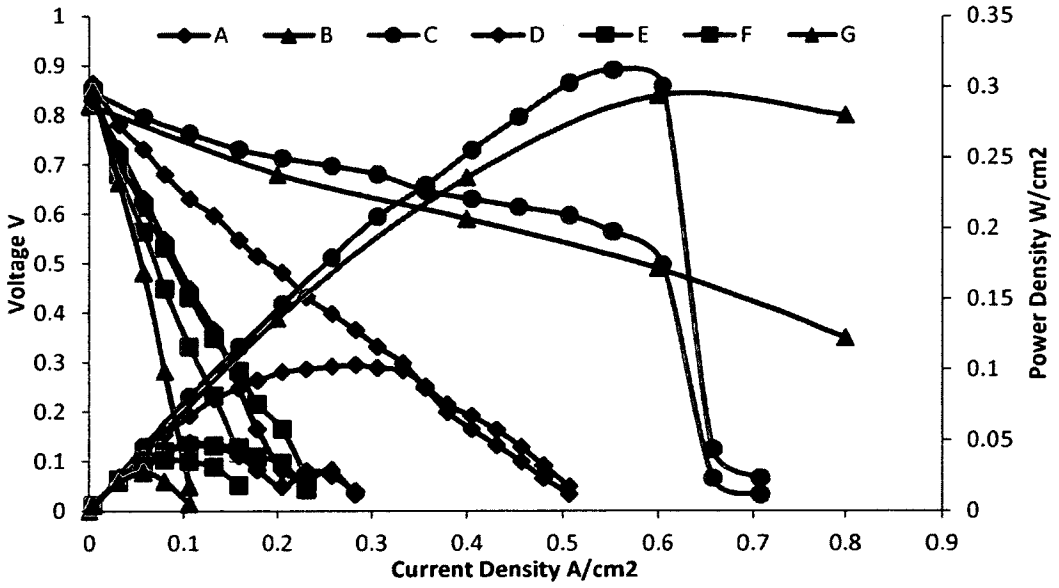

Figure 5.20: H2 Power Curves for MEA component troubleshooting Anode/Cathode GDL=Toray. Fuel Cell T=65C, Anode loading: 0.4mg/cm2 Pt, Cathode loading 0.4mg/cm2 Pt, Anode/Cathode Humidification T=75C, 2x Stoich H2, 3x Stoich Air. N-112 Membrane.
Note: The lettering of the curves does not correspond to Table 5.3.

Figure 5.20 shows the power curves for tests performed over several months. To check potential causes for the poor performance, each component of MEA preparation is systematically altered and tested. A control test using a commercial MEA (0.5mg/cm^2 Pt loading) is performed and shown in Figure 5.2 as Curve C. The positive result confirms the fuel cell system is not the source of the reduced performance. With the system validated, each material used in MEA fabrication came into question; new 20% Pt, commercial platinum catalyst is purchased and MEAs prepared(Curve D); new Nafion membrane is purchased and prepared(Curve E); the Nafion ionomer solution used in the catalyst ink is replaced(curve F), and new Toray GDL is purchased(Curve G). Finally the DI water source is changed. The curve, B shows the effect of changing the water source from DI tap in the lab to DI water supplied from a separate system in the Engineering building on campus. The results nearly match the commercial MEA in terms of peak performance.

The degraded performance is either due to the fact that the membranes used in the repeatability test verification are prepared and stored prior to the study, or that the DI source in the study became contaminated. Either the DI water in the preparation for the membranes is sourced somewhere else, or the DI in the lab may have become contaminated over time.

5.4 Conclusions

The research work in this study successfully established a catalyst synthesis procedure for use with DAFCs. The study reports the results of 6 synthesized catalysts for DAFC use. Those catalysts are 6 of 49 individual batches of catalysts prepared over the course of this study. Table 5.5 lists all of the catalysts prepared.

Table 5.5: Catalysts Synthesized

Catalyst	Number of Prepared Samples
Pt/C	18
Pd/C	6
Pt_xSn_y/C	15
$Pt_xSn_yRu_z/C$	8
Pt_xPd_y/C	2

Single fuel cell test results from the MEAs prepared with the 6 catalysts provide the following conclusions:

1.) The fuel cell apparatus works satisfactorily with the addition of an automated syringe pump. The accuracy of the apparatus is confirmed through validation against results from a previous study done at the University of New Hampshire on the same test stand [2].

2.) This study provides a good understanding of fuel cell catalysis through successful implementation of a catalyst synthesis procedure.

3.) The prepared MEAs are very sensitive to contaminants present in the materials used to prepare them. The small scale of the single cell

architecture in this study makes the preparation an art, rather than a step by step procedure.

4.) The platinum loading of 1mg/cm^2 per electrode is necessary for DAFC use, but the metal loading of the catalyst, 20%Pt, is too low, and created preparation issues. Specifically, application of the catalyst to the GDL is made more difficult by poor adhesion, cracking and flaking of the drying catalyst layer due to its increased thickness.

5.) At flow rates of 1ml/min EtOH Catalyst B (PtSn 1:1), D (PtSnRu/C 1:1:0.5), and F (PtSnRu/C 1:0.5:0.5), show lowest performance at a high temperature of 85°C. The relationship between temperature and flowrate is inversed for some individual catalysts at 2ml/min EtOH flow rates. In this case high temperature is directly related to higher performance.

6.) Catalysts are randomly sensitive to changes in flow rates. Variability in the MEA behavior with respect to flow rate is likely due to the variability in the catalyst layer thickness.

7.) The DI water used in this study may be contaminated and produced ineffective MEAs.

8.) Contamination likely altered results and prevented a clear comparison of the binary and ternary catalyst composition from being made. As a result, the peak fuel cell power output for the synthesized catalysts tested only varied by ~5mW/cm^2.

5.5 Recommendations

1.) Future work should consider any of the DAFC catalysts that show an increased activity toward ethanol electrooxidation over platinum, specifically Pt_2Sn/C. The focus should be to optimize catalyst compositions for use in a DAFC.

2.) Based on the literature, the activity of Pd in alkaline solutions for ethanol electrooxidation is very high. Pd based electrocatalysts should be further investigated for use in a DAFC.

3.) Novel catalyst supports, such as carbon nanotubes and graphene, while not economically practical, should be evaluated for DAFC use.

4.) An in depth study of the anodic reactions in a DAFC using gas chromatography to determine product yield and selectivity is recommended. This would help to determine the binary or ternary catalyst composition with the highest activity toward complete electrooxidation of ethanol.

5.) It would be prudent to test all the remaining catalyst samples from this study in a half cell. The half cell tests would serve as validation for the synthesis method used in this study. It would also be advantageous to test each potential catalyst in a half cell prior to single cell testing given the availability of both facilities at UNH.

6.) A synthesis method to deposit palladium on carbon should be investigated. Once a synthesis method is available, binary and ternary catalysts based on Pd, Pt, Sn and Ru should be studied for their effectiveness for ethanol electrooxidation.

7.) For each catalyst, characterization should be performed. Given the limited accuracy of the XPS test initially attempted, it would be advisable to seek additional methods(elemental analysis, surface area, TGA, etc.) for complete catalyst characterization.

8.) MEA optimization should be performed. At present, much of the work on direct alcohol fuel cells revolves around developing effective catalysts. No work has been done on determining the most effective membrane and GDL combinations for DAFC use. Given the previous work at UNH that found micro porous layers to effectively increase DMFC performance [2], GDLs with various MPL loadings and wet proofing would be the best place to start.

9.) MEA preparation should be improved. As in industry, incorporation of a screen printing, decal pressing or a spray technique to apply catalyst directly to the membrane, should be investigated for MEA preparation.

10.) With successful tests in a $5cm^2$ cell, scale up tests should be performed using the $50cm^2$ fuel cell fixture available in the lab. While costly, it would ensure performance scales up to active area geometries common in industry.

11.) In industry, conditioning is done through current cycling. Implementation of such cycling would produce results much more appropriate for comparison to other studies or results from industry.

12.) A conductivity meter should be used to determine the conductivity of the DI water in both the system humidifiers and in the preparation materials. This is a common practice in research and industry labs and would help to reduce a possible source of contamination.

13.) Platinum loading on carbon should be increased for cases where high Pt/cm^2 loading is required. This would reduce the thickness of the catalyst layer, and the total amount of material needed to achieve the loadings required.

14.) A study on non-platinum catalysts and catalysts with very low platinum content should be performed to focus on reduction of catalyst cost.

15.) Impedance analysis should be performed on the cell to understand the relationship between catalyst layer thickness, carbon and Pt loading, ohmic overpotential, contact and diffusion resistance in the cell. This is common practice in industry, and an incredibly important tool for analysis and understanding of results.

Chapter 6 : References

[1] Larminie J, Dicks A, "Fuel Cell Systems Explained", John Wiley and Sons, NY, USA, 1999.

[2] Morgan, Jason, "Study of Gas Diffusion Layers in Direct Methanol Fuel Cells(DMFC)", Masters Thesis, University of New Hampshire, 2008.

[3] Hydrogen, Methanol and Ethanol Energy densities, http://hypertextbook.com

[4] Bergamaski K, Gonzalez E.R, Nart F.C, "Ethanol oxidation on carbon supported platinum-rhodium bimetallic catalysts", Electrochimica Acta, Vol. 53, 4396-4406, 2008.

[5] Wu G, Swaidan R, Cui G, "Electrooxidations of ethanol, acetaldehyde and acetic acid using PtRuSn/C catalysts prepared by modified alcohol-reduction process", Journal of Power Sources, Vol.172, 180-188, 2007.

[6] Spinacé E.V, Neto A.O, Vasconcelos T, Linardi M, "Direct ethanol fuel cells based on PtSn anodes: the effect of Sn content on the fuel cell performance", Journal of Power Sources, Vol. 137, 17-23, 2004.

[7] Rousseau S, Coutanceau C, Lamy C, Léger J.-M, "Direct ethanol fuel cell (DEFC): Electrical performances and reaction products distribution under operating conditions with different platinum-based anodes", Journal of Power Sources, Vol. 158, 18-24, 2006.

[8] Suffredini H.B, Tricoli V, Vatistas N, Avaca L.A, "Electro-oxidation of methanol and ethanol using a Pt–RuO2/C composite prepared by the sol–gel technique and supported on boron-doped diamond", Journal of Power Sources, Vol. 158, 124-128, 2006.

[9] Xu C, Shen P.K, Liu Y, "Ethanol electrooxidation on Pt/C and Pd/C catalysts promoted with oxide", Journal of Power Sources, Vol. 164, 527-531, 2007.

[10] Neto A.O, Dias R.R, Tusi M.M, Linardi M, Spinacé E.V, "Electro-oxidation of methanol and ethanol using PtRu/C, PtSn/C and PtSnRu/C electrocatalysts prepared by an alcohol-reduction process", Journal of Power Sources, Vol. 166, 87-91, 2007.

[11] Wu G, Swaidan R, Cui G, "Electrooxidations of ethanol, acetaldehyde and acetic acid using PtRuSn/C catalysts prepared by modified alcohol-reduction process", Journal of Power Sources, Vol 172, 180-188, 2007.

[12] Hu F, Chen C, Wang Z, Wei G, Shen P.K, "Mechanistic study of ethanol oxidation on Pd–NiO/C electrocatalyst", Electrochimica Acta, Vol. 52, 1087-1091, 2006.

[13]Chorkendorff I, Niemantsverdriet J.W, "Concepts of Modern catalysis and Kinetics", 2007. Wiley-VCH.

[14] Kim J. H, Choi S.M, Nam S.H, Seo M.H Choi S.H, Kim W.B, "Influence of Sn content on PtSn/C catalysts for electrooxidation of C1–C3 alcohols: Synthesis, characterization, and electrocatalytic activity", Applied Catalysis B Environment, Vol. 82, 89-102, 2008.

[15] Zhou W.J, Song S.Q, "Direct ethanol fuel cells based on PtSn anodes: the effect of Sn content on the fuel cell performance", Journal of Power Sources, Vol. 140, 50-58, 2005.

[16] Antolini E, "Catalysts for direct ethanol fuel cells", Journal of Power Sources, Vol. 170, 1-12, 2007.

[17] Wang H, Jusys Z, Behm R.J, "Ethanol electro-oxidation on carbon-supported Pt, PtRu and Pt3Sn catalysts: A quantitative DEMS study", Journal of Power Sources, Vol. 154, 351-359, 2006.

[18] Simões F.C, Anjos D.M, Vigier F, Léger J.-M, Hahn F, Coutanceau C, Gonzalez E.R, Tremiliosi-Filho G, Andrade A.R, Olivi P, Kokoh K.B, "Electroactivity of tin modified platinum electrodes for ethanol electrooxidation", Journal of Power Sources, Vol.167, 1-10, 2007.

[19] Colmati F, Antolini E, Gonzalez E.R, "Effect of temperature on the mechanism of ethanol oxidation on carbon supported Pt, PtRu and Pt3Sn electrocatalysts ", Journal of Power Sources, Vol. 157, 98-103, 2006.

[20] Guo Y, Zheng Y, Huang M, "Enhanced activity of PtSn/C anodic electrocatalyst prepared by formic acid reduction for direct ethanol fuel cells", Electrochimica Acta, Vol. 53, 3102-3108, 2008.

[21] Xue X, Ge J, Tian T, Liu C, Xing W, Lu T, "Enhancement of the electrooxidation of ethanol on Pt–Sn–P/C catalysts prepared by chemical deposition process", Journal of Power Sources, Vol. 172, 560-569, 2007.

[22] Bagchi J, Bhattacharya S.K, "The effect of composition of Ni-supported Pt-Ru binary anode catalysts on ethanol oxidation for fuel cells", Journal of Power Sources, Vol. 163, 661-670, 2007.

[23] Liu Z, Ling X.Y, Su X, Lee J.Y, Gan L.M, "Preparation and characterization of Pt/C and PtRu/C electrocatalysts for direct ethanol fuel cells ", Journal of Power Sources, Vol. 149, 1-7, 2005.

[24] Tsiakaras P.E, "PtM/C (M = Sn, Ru, Pd, W) based anode direct ethanol–PEMFCs: Structural characteristics and cell performance", Journal of Power Sources, Vol. 171, 107-112, 2007.

[25] Gupta S.S, Datta J, "Electrode kinetics of ethanol oxidation on novel CuNi alloy supported catalysts synthesized from PTFE suspension ", Journal of Power Sources, Vol. 145, 124-132, 2005.

[26] Bergamaski K, Gonzalez E.R, Nart F.C, "Ethanol oxidation on carbon supported platinum-rhodium bimetallic catalysts", Electrochimica Acta, Vol. 53, 4396-4406, 2008.

[27] Frano Barbir, "PEM Fuel Cells Theory and Practice", Elsevier Academic Press, MA, USA, 2005.

[28] Gamburzev S, John Appleby A, "Recent progress in performance improvement of the proton exchange membrane fuel cell (PEMFC)", Journal of Power Sources, Vol. 107, 5-12, 2002.

[29] Li G, Pickup, P.G, "Analysis of performance losses of direct ethanol fuel cells with the aid of a reference electrode", Journal of Power Sources, Vol.161, 256-263, 2006.

[30] Kontou S, Stergiopoulos V, Song S, P. Tsiakaras, "Ethanol/water mixture permeation through a Nafion® based membrane electrode assembly", Journal of Power Sources, Vol. 171, 1–7, 2007.

[31] Zaidi S.M.J., Mikhailenko S.D., Robertson G.P., Guiver M.D., Kaliaguine S, "Proton conducting composite membranes from polyether ketone and heteroplyacids for fuel cell applications", Journal of Membrane Science, Vol. 173, 17-34, 2000.

[32] Smitha B, Sridhar S, Khan A.A., "Synthesis and Characterization of Poly(vinyl alcohol)-Based Membranes for Direct Methanol Fuel Cell", Journal of Applied Polymer Science, Vol. 95, 1154-1163, 2005.

[33] Xie X, Mao Z, Xu J, "A Hybride Membrane of Modified Polybenzimidazole and Heteropoly Acid for Direct Methanol Fuel Cell", Power System Technology, Vol. 1, 13-17, Oct 2002.

[34] Guo Q, Pintauro P.N., Tang H, O'Connor S, "Sulfonated and crossinked polyphospazene-based proton-exchange membranes", Journal of Membrane Science, Vol. 154, 175-181, 1999.

[35] Park G, Sohn Y, Yang T, Yoon Y, Lee W, Kim C, "Effect of PTFE contents in the gas diffusion media on the performance of PEMFC", Journal of Power Sources, Vol. 131, 182-187, 2004.

[36] Giorgi L, Antolini E, Pozio A, Passalacqua E, "Influence of the PTFE content in the diffusion layer of low-Pt loading electrodes for polymer electrolyte fuel cells", Electrochimica Acta, Vol. 43, No. 24, 3765-3680, 1998.

[37] Prasanna M, Ha H. Y, Cho E. A, Hong S, Oh I, "Influence of Cathode Gas Diffusion Media on the Performance of the PEMFCs", Journal of Power Sources, Vol. 131, 147-154, 2004.

[38] Moreira J, Sebastian P.J., Ocampo A. L., Castellans R. H., Cano U, Salazar M.D., "Dependence of PEM Fuel Cell Performance on the Configuration of the Gas Diffusion Electrodes", Journal of New Materials for Electrochemical Systems, Vol. 5, 173-175, 2002.

[39] Lister S, McLean G, "PEM Fuel Cell Electrodes", Journal of Power Sources, Vol. 130, 61-76, 2004.

[40] Song J. M, Cha S. Y, Lee W. M, "Optimal Composition of Polymer Electrolyte Fuel Cell Electrodes Determined by the AC impedance Method", Journal of Power Sources, Vol. 94, 78-84, 2001.

[41] Qi Z, Kaufman A, "Improvement of Water Management by a Microporous Sublayer for PEM Fuel Cells", Journal of Power Sources, Vol. 109, 38-46, 2002.

[42] Wakizoe M, Velev O.A., Srinivasan S, "Analysis of Proton Exchange Membrane Fuel Cell Performance With Alternate Membranes", Electrochimica Acta, Vol. 40, 335-344, 1995.

[43] Barragan V.M., Ruiz-Bauza C, Villaluenga J.P.G., Seoane B, "Transport of methanol and water through Nafion membranes", Journal of Power Sources, Vol. 130, 22-29, 2004.

[44] Song S, Zhou W, Tian J, Chai Rui, Sun G, Xin Q, Kontoi S, Tsiakaras P, "Ethanol crossover phenomena and its influence on the performance of DEFC", Journal of Power Sources, Vol.145, 266-271, 2005.

[45] Wilson M.S, Gottesfeld S,"Thin-film catalyst layers for polymer electrolyte fuel cell electrodes", Journal of Applied Electrochemistry, Vol. 22, 1-7, 1992.

[46] Makino K, Furukawa K, Okajima K, Sudoh M,"Performance of sputter-deposited platinum cathodes with Nafion and carbon loading for direct methanol fuel cells", Journal of Power Sources, Vol. 166, 30-34,2007.

[47] EG&G Services, Parsons, Inc., Science Applications International Corporation, "Fuel Cell Handbook", US Department of Energy Office of Fossil Energy, VA, USA, 2000.

[48] Zhang Y, Zhang H, Zhai Y, Zhu X, Bi Cheng, " Investigation of Self-humidifying membranes based on sulfonated poly(ether ether ketone) hybrid with sulfated xirconia supported Pt catalyst for fuel cell applications", Journal of Power Sources, Vol. 168, 323-329, 2007.

[49] Koppola, Karuna, "Study of Gas Diffusion Layers in PEM Fuel Cells", Masters Thesis, University of New Hampshire, 2004.

[50] Lima F.H.B, Gonzalez E.R, "Electrocatalysis of ethanol oxidation on Pt monolayers deposited on carbon-supported Ru and Rh nanoparticles", Applied Catalysis B: Environmental, Vol. 79, 341-346, 2008.

[51] Xu C, Shen P.K, "Electrochamical oxidation of ethanol on Pt-CeO2/C catalysts", Journal of Power Sources, Vol. 142, 27-29, 2005.

[52] Calegaro M.L, Suffredini H.B, Machado S.A.S, Avaca L.A, "Preparation, characterization and utilization of a new electrocatalyst for ethanol oxidation obtained by the sol–gel method ", Journal of Power Sources, Vol. 156, 300-305, 2006.

[53] Wang Z, Yin G, Zhang J, Sun Y, Shi P, "Investigation of ethanol electrooxidation on a Pt–Ru–Ni/C catalyst for a direct ethanol fuel cell", Journal of Power Sources, Vol. 160, 37-43, 2006.

[54] Zheng H.T, Li Y, Chen S, Shen P.K, "Effect of support on the activity of Pd electrocatalyst for ethanol oxidation", Journal of Power Sources, Vol. 163, 371-375, 2006.

[55] Hu F, Ding F, Song S, Shen P.K, "Pd electrocatalyst supported on carbonized TiO2 nanotube for ethanol oxidation", Journal of Power Sources, Vol. 163, 415-419, 2006.

[56] Huang M, Wang F, Li L, Guo Y, "A novel binary Pt3Tex/C nanocatalyst for ethanol electro-oxidation", Journal of Power Sources, Vol. 178, 48-52, 2007.

[57] Hu F.P,Wang Z, Li Y, Li C, Zhang X, Shen P.K, "Improved performance of Pd electrocatalyst supported on ultrahigh surface area hollow carbon spheres for direct alcohol fuel cells", Journal of Power Sources, Short Communication, Vol. 177, 61-66, 2008.

[58] Li G, Pickup, P.G, "The promoting effect of Pb on carbon supported Pt and Pt/Ru catalysts for electro-oxidation of ethanol", Electrochimica Acta, Vol. 52, 1033-1037, 2006..

[59] Mozingo R, "Organic Synthesis Collective Volume 3", 1955. John Wiley & Sons.

[60] Yuan H, Guo D, Qiu X, Zhu W, Chen L, "Influence of metal oxides on Pt catalysts for methanol electrooxidation using electrochemical impedance spectroscopy", Journal of Power Sources, Vol.188, 8-13, 2009.

[61] Bard A, Faulkner L, "Electrochemical Methods: Fundamentals and Applications", 2000. Wiley.

[62] Babu P.K, Chung J.-H, Oldfield E, Wieckowski A, "CO surface diffusion on platinum fuel cell catalysts by electrochemical NMR", Electrochimica Acta, Vol. 53, 6672-6679, 2008.

[63] Ferrin P, Nilekar A.U, Greeley J, Mavrikakis M, Rossmeisl J, "Reactivity descriptors for direct methanol fuel cell anode catalysts", Surface Science, Vol. 602, 3424-3431, 2008.

[64] Kulikovsky A.A, "Direct methanol–hydrogen fuel cell: The mechanism of functioning", Electrochemistry Communications, Vol. 10, 1415-1418, 2008.

[65] Antolini E, Lopes T, Gonzalez E.R, "An overview of platinum-based catalysts as methanol-resistant oxygen reduction materials for direct methanol fuel cells", Journal of Alloys and Compounds, Vol. 461, 253-262, 2008.

[66] Denis M.C, Lefevre M, Guay D, Dodelet J.P, "Pt-Ru catalysts prepared by high energy ball-milling for PEMFC and DMFC: Influence of the synthesis conditions", Electrochimica Acta, Vol. 53, 5142-5154, 2008.

[67] Yoo E, Okada T, Kizuka T, Nakamura J, "Effect of carbon substrate materials as a Pt–Ru catalyst support on the performance of direct methanol fuel cells", Journal of Power Sources, Vol. 180, 221-226, 2008.

[68] Song H, Qiu X, Li F, "Effect of heat treatment on the performance of TiO2-Pt/CNT catalysts for methanol electro-oxidation", Electrochimca Acta, Vol. 53, 3708-3713, 2008.

[69] Ham D.J, Kim Y.K, Han S.H, Lee J.S, "Pt/WC as an anode catalyst for PEMFC: Activity and CO tolerance", Catalysis Today, Vol. 132, 123-126, 2008.

[70] Baglio V, Stassi A, Di Blasi A, D'Urso C, Antonucci V, Arico A.S, "Investigation of bimetallic Pt–M/C as DMFC cathode catalysts", Electrochimica Acta, Vol. 53, 1360-1364, 2007.

[71] Maillard F, Bonnefont A, Chatenet M, Guetaz L, Doisneau-Cottignies B, Roussel H, Stimming U, "Effect of the structure of Pt–Ru/C particles on COad monolayer vibrational properties and electrooxidation kinetics", Electrochimica Acta, Vol. 53, 811-822, 2007.

[72] Zheng J, Lee J.Y, "Ruthenium-free, carbon-supported cobalt and tungsten containing binary & ternary Pt catalysts for the anodes of direct methanol fuel cells", Int. Journal of Hydrogen Energy, Vol. 32, 4389-4396, 2007.

[73] Jeon M.K, Daimon H, Lee K.R, Nakahara A, Woo S.I, "CO tolerant Pt/WC methanol electro-oxidation catalyst", Electrochemistry Communications, Vol. 9, 2692-2695, 2007.

[74] Jeon M.K, Won J.Y, Lee K.R, Woo S.I, "Highly active PtRuFe/C catalyst for methanol electro-oxidation", Electrochemistry Communications, Vol. 9, 2163-2166, 2007.

[75] Antolini E, "Platinum-based ternary catalysts for low temperature fuel cells: Part I. Preparation methods and structural characteristics", Applied Catalysis B Environment, Vol. 74, 324-336, 2007.

[76] Antolini E, "Platinum-based ternary catalysts for low temperature fuel cells: Part II. Electrochemical properties", Applied Catalysis B Environment, Vol. 74, 337-350, 2007.

[77] Viswanathan B, "Architecture of carbon support for Pt anodes in direct methanol fuel cells", Catalysis Today, Vol. 141, 52-55, 2009.

Appendix A : Reactant Flow Rates

Molar flow rates for all reactants in this study were determined by:

$$n = \frac{I}{zF},$$

where *n*, *I*, *z* and *F* are the molar flow rate in mol/min, the current density in A/cm^2, the reaction charge number and Faraday's constant, respectively. The molar flow rates of H_2, O_2, and ethanol are then given by:

$$n_{H_2} = \frac{I}{2F},$$
$$n_{O_2} = \frac{I}{2F},$$
$$n_{EtOH} = \frac{I}{6F}$$

To sufficiently supply the fuel cell with fuel and oxidants, H_2 and ethanol are supplied at 2 times the stoichiometric requirement and O_2 at 3 times. A sample calculation for ethanol flow(2x stoich) required for 1 A/cm^2 in a 5cm^2 fuel cell is given by the following:

$$n_{EtOH} = \frac{1}{6 \times 96485} = 1.727 \times 10^{-6}\, mol/s = 1.04 \times 10^{-4}\, mol/min\,,$$

Given the molecular weight of ethanol to be 46.068g/mol and its density at STP to be 0.789 g/mL, the flow rate can be expressed in mL/min at STP:

$$v_{EtOH} = 0.0061 mL/min$$

For a 5cm^2 cell and a 2x stoich, the required flow rate is:

$$v_{EtOH} = 0.0061 \times 5 \times 2 = 0.061 mL/min$$

The flow rate determined above is for pure ethanol, the actual required flow rates for a 1M EtOH solution at 2x stoich are given in Table A1.

Table A.1: Reactant Flow Rates

Total Current A	Current Density A/cm^2	H2 Flow Rate 2x Stoich cm^3/min	Oxygen Flow Rate 3x Stoich cm^3/min	Air Flow Rate 3x Stoich cm^3/min	Ethanol 2x Stoich mL/min	Ethanol Solution 2x Stoich mL/min
0.5	0.1	7	10	50	0.006	0.104
1	0.2	14	21	100	0.012	0.208
1.5	0.3	21	31	149	0.018	0.312
2	0.4	28	42	199	0.024	0.415
2.5	0.5	35	52	249	0.030	0.519
3	0.6	42	63	299	0.036	0.623
3.5	0.7	49	73	348	0.042	0.727
4	0.8	56	84	398	0.048	0.831
4.5	0.9	63	94	448	0.055	0.935
5	1	70	104	498	0.061	1.039
5.5	1.1	77	115	547	0.067	1.143
6	1.2	84	125	597	0.073	1.246

Appendix B : Catalyst Loading & Synthesis Sample Calculation

To determine the mass of precursors for synthesis, the following relationships are used.

$$Target\ total\ Catalyst\ Mass(g) \times \frac{Target\ Pt\ \ Weight\ \%}{100}$$

$$= Target\ Pt\ Catalyst\ Mass(g)$$

$$\frac{Precursor\ Molecular\ weight(g/mol)}{Pt\ Molecular\ weight(g/mol)} = weight\ fraction\ of\ Pt\ in\ precursor$$

$$\frac{Target\ Pt\ Catalyst\ Mass(g)}{weight\ fraction\ of\ Pt\ in\ precursor} = total\ mass\ precursor\ required(g)$$

For binary or ternary catalyst synthesis, the non-Pt catalyst precursor required is determined by the following relationship.

$$\frac{Target\ Pt\ Catalyst\ Mass(g)}{Pt\ Molecular\ Weight(g/mol)} \times \frac{Moles\ binary\ metal}{Moles\ Pt}$$

$$\times\ Molecular\ weight\ of\ binary\ Metal$$

$$= Target\ binary\ metal\ mass(g)$$

The same steps used to determine the Pt precursor required is applied to the binary and ternary metals for determining precursor requirements. The

Carbon support required is simply the total target mass of catalyst required less the mass of each catalyst metal.

A sample calculation to determine the precursors required to prepare 0.06g of Pt_2Sn/C with 20wt% Pt is provided:

Chloroplatinic Acid(H_2PtCl_6-$6H_2O$) Molecular weight : 517.9 g/mol

Platinum Molecular weight: 195.1 g/mol

Tin Chloride($SnCl_2$) Molecular weight : 225.63 g/mol

Tin Molecular weight: 118.71 g/mol

$$0.06g \times 0.2 = 0.012g\ Pt$$

$$\frac{517.9\ g/mol}{195.1\ g/mol} = 0.3767\ wt\ fraction\ Pt\ in\ Precursor$$

$$\frac{0.012g\ Pt}{0.3767} = 0.03185g\ Chloroplatinic\ Acid$$

$$\frac{0.012g\ Pt}{195.1\ g/mol} \times \frac{1\ Mol\ Sn}{2\ Moles\ Pt} \times 118\frac{g}{mol} = 0.00365g\ Tin$$

$$\frac{225.63\ g/mol}{118.71\ g/mol} = 0.526\ wt\ fraction\ Tin\ in\ Precursor$$

$$\frac{0.00365g\ Sn}{0.526} = 0.03185g\ Tin\ Chloride$$

$$0.06 - 0.012 - 0.00365 = 0.044g\ Carbon\ Support$$

To determine the loading of the catalyst on each electrode, the dry GDL weight was subtracted to the final coated weight of the GDL. The following is

sample data for Pt_2Sn/C MEA preparation (Nafion:Catalyst ratio assumed constant) :

Pt_2Sn/C mass: 0.025g

Nafion(10%): 0.0962

Catalyst as a % of dry weight added: 72.2%

Active Area: $5cm^2$

Dry GDL Weight: 0.0643g

Coated GDL Weight: 0.0984g

Dry Mass added to GDL = 0.0984 - 0.0643 = 0.0341g

Total Catalyst on GDL= 0.0341 x 0.722 = 0.0246g

Pt Catalyst Loading = (0.0246 x 0.2) / 5 = 0.985 g/cm^2

Nafion Loading in catalyst layer = [0.0341 x (1 - 0.722)] / 5 = 1.37 g/cm^2

The Pt loading is calculated to be approximately $1mg/cm^2$, the target loading. This loading was achieved for all DAFC catalysts in the study.